EFFECT OF INORGANIC FILLER SIZE ON NANOCOMPOSITE ION EXCHANGE MEMBRANES FOR SALINITY GRADIENT POWER GENERATION

A Master's Thesis
Presented to
The Academic Faculty

by

Shira Molly Glabman

In Partial Fulfillment
of the Requirements for the Degree
Master of Science in the
School of Civil and Environmental Engineering

Georgia Institute of Technology
December 2014

EFFECT OF INORGANIC FILLER SIZE ON NANOCOMPOSITE ION EXCHANGE MEMBRANES FOR SALINITY GRADIENT POWER GENERATION

Approved by:

Dr. Yongsheng Chen, Advisor
School of Civil and Environmental Engineering
Georgia Institute of Technology

Dr. John Crittenden, Committee Member
School of Civil and Environmental Engineering
Georgia Institute of Technology

Dr. Ching-Hua Huang, Committee Member
School of Civil and Environmental Engineering
Georgia Institute of Technology

Date Approved: November 6, 2014

ACKNOWLEDGEMENTS

I wish to especially thank my mother and father. If it were not for their support, I would not have the opportunity to be at Georgia Tech writing this thesis. I would also like to thank my sister, who is my role model and has always been an infinite source of guidance. Last, I owe a heartfelt thanks to my fiancé for constantly providing me with a myriad of words of wisdom and kindness.

Thank you to my advisor, Dr. Yongsheng Chen, my research partner, Jin Gi Hong, my reading committee members, and my university, Georgia Institute of Technology, without which this project would have been impossible.

TABLE OF CONTENTS

LIST OF TABLES

LIST OF FIGURES

LIST OF SYMBOLS

C_{NaOH}	Concentration of Sodium Hydroxide
C_{fix}	Fixed Charge Density
μ	Micron
α	Permselectivity
R_{sol}	Resistance of Blank Test
R_{cell}	Resistance of Cell
R_{mem}	Resistance of Membrane
V_{NaOH}	Volume of Sodium Hydroxide
W/m^2	Watt per square meter
W_{dry}	Weight of the Dry Membrane
W_{wet}	Weight of the Wet Membrane

LIST OF ABBREVIATIONS

AEM	Anion Exchange Membrane
CD	Charge Density
CEM	Cation Exchange Membrane
DI	De-Ionized
DMSO	Dimethylsulfoxide
EDS	Energy-Dispersive X-Ray Spectroscopy
FTIR	Fourier Transform Infrared
HCl	Hydrogen Chloride
Hz	Hertz
IEC	Ion Exchange Capacity
IEM	Ion Exchange Membrane
NaCl	Sodium Chloride
NaOH	Sodium Hydroxide
PPO	Poly (2,6-dimethyl-1,4-phenylene oxide)
PRO	Pressure-Retarded Osmosis
PVA	Polyvinyl Alcohol
PVC	Polyvinylchloride
RED	Reverse Electrodialysis
SD	Swelling Degree
SEM	Scanning Electron Microscopy
SiO_2	Silicon Dioxide/Silica
sPPO	Sulfonated poly (2,6-dimethyl-1,4-phenylene oxide)

TEM	Transmission Electron Microscopy
TW	Terawatt
UV	Ultraviolet
V	Volts

SUMMARY

Recovering energy from the ocean using the salinity gradient power obtained from the reverse electrodialysis (RED) process has great potential to meet the world's growing energy demand, while also cutting down on greenhouse gas emissions and the use of scarce fossil fuels. Some limitations prevent RED systems from large-scale applications including high cost of membranes, slow development for natural salinity conditions, and lack of tailor-made RED membranes for salinity gradient power generation. The currently available commercial ion exchange membranes (IEMs) lack sufficient properties to generate optimal power in an RED system. Our work is focused on synthesizing ion exchange membranes specifically for an RED system. In recent years, it has been discovered that the ideal IEMs for RED have low resistance and high selectivity.

The addition of inorganic filler particles into the organic polymer matrix of cation exchange membranes (CEMs) has been shown to increase proton conductivity, hydrophilicity, and surface area. In this study, we introduce a new type of nanocomposite membranes made by incorporating sulfonated SiO_2 nanoparticles into a sulfonated poly (2,6-dimethyl-1,4-phenylene oxide) (sPPO) polymer. This work is the first time the use of SiO_2-SO_4^{2-} in the PPO polymer matrix has been reported in this field. Our purpose is to evaluate the effect of adding two different sizes of silica nanoparticles (15 nm and 70 nm) in various loading amounts (0 wt%, 0.2 wt%, 0.5 wt%, 0.8 wt%, 1 wt%) on membrane properties such as ion exchange capacity, swelling degree, membrane resistance, and permselectivity. Finally, our novel nanocomposite membranes are tested

in an RED stack to measure their power generation. The results show that SiO_2-sPPO membranes are more suitable for energy generation by RED than commercially-available CEMs. More specifically, the most favorable physical and electrochemical characteristics are exhibited with the membrane containing 0.5 wt% SiO_2-SO_3H loading with the larger (70 nm) nanoparticles. All membranes blended with the 70 nm particles have lower area resistance and, therefore, higher gross power density than the membranes containing the 15 nm particles. The highest power density of 1.3 W/m^2 is achieved from the 0.5 wt% SiO_2-SO_3H nanocomposite membranes containing the larger sized particles.

CHAPTER 1

INTRODUCTION

1.1 Motivation for Research

Global population is rapidly increasing, in large part due to technology and medical advances. A growing world population, especially in rapidly developing countries, leads to growing energy demand and consumption per capita for daily use and development. The increasing anthropogenic need for energy and the desire to protect our environment may cause a major economic or environmental crisis in the coming years. Innovative technology using renewable sources is needed to meet our growing energy needs and reduce our anthropogenic contributions to climate change.

Current trends in energy consumption still disproportionately favor nonrenewable fossil fuel sources. According to the 2013 Key World Energy Statistics, published by the International Energy Agency, oil (31.5%), coal (28.8%), and natural gas (21.3%) still account for the majority of the fuel supply. Just 1.0% of the world's total primary energy usage came from renewable sources such as geothermal, solar, wind, and heat in 2012.[1]

In the last few decades, there have been rising concerns about the harmful impacts of climate change. A recent study has shown that a business-as-usual approach to energy consumption is unsustainable regardless of the sustainability criteria.[2] The Intergovernmental Panel on Climate Change published a landmark assessment report in 2013 stating that the business-as-usual model leads to runaway climate change and global warming, ultimately resulting in sea level rises and extreme weather conditions.[3] Compounding the issue is the imminent scarcity of fossil fuels.

Fossil fuel consumption unavoidably causes carbon dioxide (CO_2) emissions. As the leading contributor of CO_2 in the atmosphere, fossil fuel combustion produces 30 gigatons of CO_2 annually.[4] Reduction in the negative effects of climate change can only be achieved through a drastic reduction in fossil fuel usage. Implementing novel renewable energy technologies in place of fossil fuels will have the most significant payout for a similar investment of resources.

Current renewable energy resources, in order of their theoretical potential, include solar (photovoltaics and concentrators), wind, enhanced geothermal, hydropower, and biopower. Some limitations contributing to the lack of implementation of renewable energy systems are inadequate investments in new technologies, slow states of development, and scale-ups needed for sufficient power production.

One of the most expansive and largely unharnessed energy comes from the ocean. This so-called blue energy, or salinity gradient power, is the free energy available from mixing water streams with different ionic concentrations, like salt water (seawater) and fresh water (river water). Salinity gradient power is available globally wherever river water flows into seawater (e.g., estuary). The estimated potential power of worldwide salinity gradient power from oceanic and river water mixing is 2.6 TW, when total discharge of all river water streams are considered.[5] Blue energy and other renewable energy sources have the potential to meet our growing energy demand with a lasting source of energy and a reduction in global greenhouse gas emissions. The National Renewable Energy Laboratory concluded that with a more flexible electric system, commercially available renewable energy sources can supply 80% of the total electricity generation for the US in 2050.[6]

Two techniques are available to harvest the alternative, renewable, and sustainable salinity gradient power into electric power: pressure-retarded osmosis (PRO) and reverse electrodialysis (RED). PRO extracts power from permeating water of a low salinity feed solution through an osmotic membrane to a pressurized, high salinity draw solution, thereby converting osmotic pressure into hydrostatic pressure which, when applied to a turbine, can generate electricity. RED, driven by the Nernst potential, uses ion selective membranes to transport cations and anions in the water to produce electrical current. The method employed in this thesis to extract this clean blue energy was reverse electrodialysis. RED was chosen due to better power generation using seawater and river water compared with PRO.[7]

There are some major advantages of RED in terms of power generation. Since runoff is relatively continuous throughout the various seasons, power generation is consistent (especially compared with wind or solar energy). Also, the immensity of the ocean provides an enormous energy resource. Last, given that salinity gradients between two natural water bodies are essentially driven by solar energy evaporating ocean water keeping it highly concentrated, there is no fuel needed to power the inflow of saline and dilute water, resulting in a net zero CO_2 emission from the RED process.

However, there are several obstacles to overcome before RED can be feasibly applied to large-scale operations. Membrane cost is relatively high leading to a high capital cost, pretreatment of input water may be necessary since membrane fouling and stability could present major problems in natural salinity conditions, stack design should be modified to be more efficient, and membranes should be optimized specifically for RED. The latter, in the opinion of our group, is the most important obstacle to consider

for successful RED systems. A recent publication also concluded that technological innovations in the ion exchange membranes (IEMs) used for RED are of utmost importance to achieve greater efficiency and higher power density performance.[8]

In many publications, there is debate about the theoretical maximum power density that can be obtained from IEMs. According to one source, the best theoretical power density that can be expected from cation exchange membranes (CEMs) is above 4 W/m^2.[9] Another group estimates that the maximum power density obtained from the available technology is 2.7 W/m^2, but that the calculated net power density with membrane resistance and cell length improvements is close to 20 W/m^2.[10] Current RED system modifications primarily aimed at improving intermembrane distance and feedwater flow rate have achieved the highest reported power density to date at 2.2 W/m^2.[11] The only way to get closer to the theoretical maximum power densities from RED technology is to make improvements in the IEMs used in the stack.

After an extensive literature review, it became evident that research aimed at synthesizing tailor-made RED membranes for this specific application was limited. Part of the reason is that the membrane properties that most contribute to high RED power output are just beginning to be understood, which makes it difficult to customize the membranes. Only recently have researchers found that low resistance and high selectivity are the key factors to optimizing IEMs for RED performance.[12]

Several studies have explored the use of various inorganic filler particles in fuel cell and desalination membrane technology.[13,14] Organic-inorganic composite IEMs have been shown to retain the beneficial properties of each component (i.e., polymer and inorganic filler) when blended. The beneficial properties of organic materials are

structural flexibility, convenient processing, tunable electronic properties, photoconductivity, efficient luminescence, and the potential for semiconducting and even metallic behavior. Inorganic compounds provide the potential for high carrier mobilities, band gap tunabilities, a range of magnetic and dielectric properties and thermal and mechanical stability.[15] These translate to high ion exchange potential, low water uptake, high conductivity, high monovalent ion selectivity, as well as high thermal and mechanical stability when both are applied to membrane development.[16] The addition of functionalized nanoparticles can facilitate enhanced ion migration with the additional pore formation in the membrane. Consequently, the area resistance of the membrane can be decreased, which is of considerable importance in RED.

Due to the crucial role of inorganic nanoparticles in forming free pores when combined with polymer matrix[17], it is necessary to understand the effect of filler particle size and loading on the membrane structure and performance in an RED application. In a previous paper from a student in our research group, novel nanocomposite membranes containing sulfonated iron (III) oxide (Fe_2O_3-SO_4^{2-}) nanoparticles in a sulfonated poly(2,6-dimethyl-1,4-phenylene oxide) (PPO) polymer matrix had favorable membrane properties and performed well in an RED stack.[18] Sulfonated functionalized silica had a substantial effect on macroscopic properties, like morphologies, physio-electrochemical performance, and stabilities of membranes for desalination applications.[19] The useful properties of PPO (e.g., high film-forming properties, good mechanical, thermal, and chemical stability, and low-moisture uptake[16, 20]) combined with the useful properties of sulfonated SiO_2 nanoparticles (e.g., hydrophilicity, ion charge transport, wide porosity,

improved conductivity, water uptake, and mechanical stability of the membranes[21]) make these materials exceptional for organic-inorganic composite membrane synthesis.

The size of inorganic fillers may alter the condition of membrane structure and pore formation, especially at the polymer-particle interfacial zone.[22] This experimental study investigates the effect of inorganic filler particle size on the structure and electrochemical performance of silica nanocomposite CEMs for RED power generation. Different inorganic particle sizes (15 nm and 70 nm) and loading amounts (0 wt%, 0.2 wt%, 0.5 wt%, 0.8 wt%, 1 wt%) were used to structurally modify the PPO polymer used to synthesize CEMs. The effect of such transformation of interfacial properties in the nanocomposites on physical and electrochemical properties was evaluated and further tested in RED stack for power production.

1.2 Energy Recovery Using Reverse Electrodialysis

The natural mixing of salt and fresh water streams leads to a change in Gibbs free energy which, through ion transport in selective RED membranes, can be liberated as electrical energy. Perfecting RED systems for large-scale operations allows us to utilize this otherwise lost free energy of mixing.

In RED, unlike electrodialysis, controlled mixing of saline and dilute solutions through membranes, produces energy. The basic principles of RED are discussed extensively in many reported studies.[7, 9, 23] An RED stack consists of any number of alternating CEMs and anion exchange membranes (AEMs) between a cathode and an anode. (Figure 1.1) As the number of membranes in the stack increases, the overall voltage production increases. For less relative power loss in the electrode system, RED stacks should have a large number of cells. Narrow compartments, formed by spacers between the membranes, are alternatively pumped with concentrated salt water and diluted fresh water. The thin spacers promote mixing between compartments and contribute to the mechanical stability of the stack. Cations migrate through the CEMs and anions migrate through the AEMs.

An electrochemical potential difference across each membrane is achieved from the salinity gradient. Cations are driven towards the cathode and anions are driven towards the anode. Redox reactions at the electrodes convert these ionic charges to electron current. When the membrane stack potential (dependent on the number of cells), or sum of cell-pair voltages, exceeds the redox potential at each electrode, the electron current can be run through electrical wires to an external electrical source to generate useful electric power.[24]

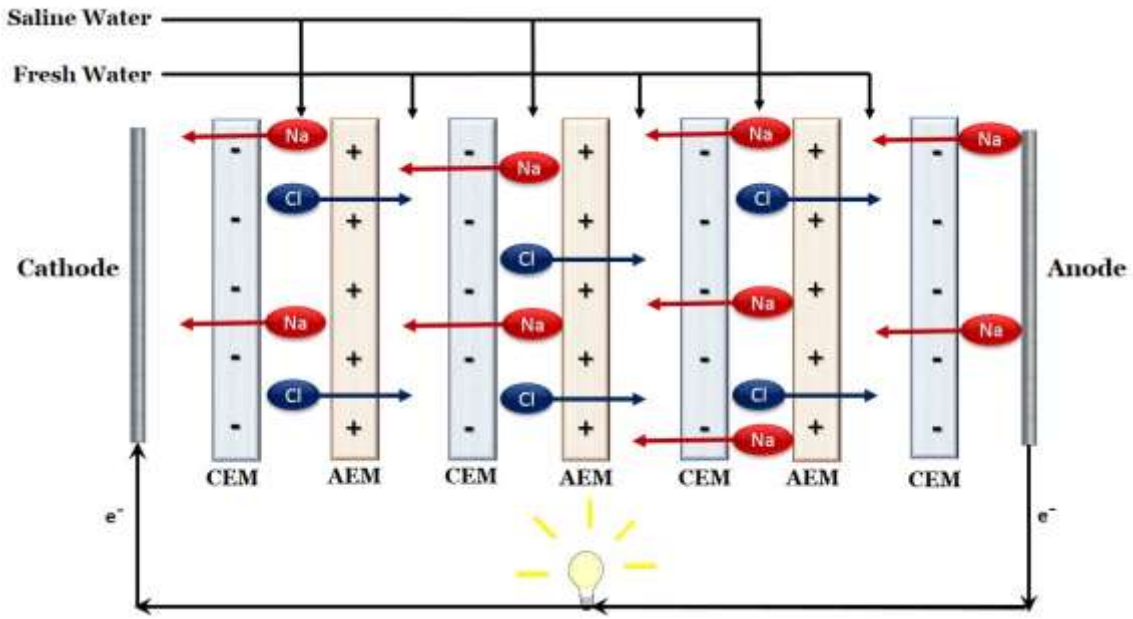

Figure 1.1 Simplified schematic of an RED stack

Summary of the basic principles of RED:

1. Feed solutions with different salt concentrations alternately through the stack.
2. Ion diffusion occurs and is regulated by IEMs, resulting in stored chemical potential energy from the ion exchange of Na^+ and Cl^- through the membranes.
3. Electron/redox transfer happens at the electrodes. Fe^{3+} is reduced to Fe^{2+} at the cathode, which is counterbalanced by the oxidation of Fe^{2+} to Fe^{3+} at the anode.
4. At the ends of the stack, an output electrical current and voltage is generated across the electrodes from the stored chemical potential energy. The current can be directly discharged as electricity if connected to an external power source (in this case, a potentiostat).

1.3 Prior and Ongoing Research

Developing low-cost IEMs with uniquely tailored electrochemical and physical properties is important for successful, sustainable energy capture from salinity gradients by RED. The currently available commercial IEMs are not ideal for RED applications due to their lack of specialized complexity. Various preparation methods and materials for RED-specific cation and anion membrane synthesis have been explored in previous work.

Homogeneous CEMs were chosen for this study over AEMs for several reasons. In general, CEMs are more thermally and chemically stable than AEMs in strongly acidic and strongly alkaline solutions; the quaternary ammonium groups in AEMs tend to decompose at elevated temperature and in concentrated alkali solutions.[25—26] CEMs have higher charge densities and higher permselectivities than AEMs due to AEM's higher swelling degree.[9] Fewer steps are required for the manufacture of CEMs.[26-27] Due to membrane structure, heterogeneous ion exchange membranes have lower charge densities and higher resistances than homogeneous membranes. Therefore, homogeneous CEMs were chosen for our purposes to produce low resistance membranes. It should be noted that although CEMs were studied here, improvements in AEMs are needed in combination with improved CEMs for more effective RED stacks. Therefore, previous experimental studies focusing on AEMs are also included in this section.

Sulfonation is a widely used chemical modification of base polymers for various membrane processes including electrodialysis, water filtration, and diffusion dialysis.[28] Sulfonation is the process whereby an electrophilic substitution takes place on the aromatic ring to increase desired charge density and hydrophilicity in the polymer matrix

(preferable for our application). By enhancing the ionic charge transfer, this modification facilitates good electrical conductivity.[29] Sulfuric acid and chlorosulfonic acid are two typical sulfonating agents, which are often used for such treatment.

For commercial applications, the most frequently used polymeric material for making CEMs is perfluorinated or partially fluorinated material. A good example of this is Nafion®, a perfluorosulfonic membrane, used almost exclusively for fuel cell technology. Nafion is very costly due to the complicated fluorochemistry required for its synthesis which, combined with its low selectivity, poor mechanical stability, and low conductivity, makes it undesirable for widespread application. Utilizing a polymer without the fluorinated species in its matrix can significantly decrease in the cost of manufacturing IEMs, and therefore, the cost of the RED technology. The non-fluorinated hydrocarbons, like poly (2,6-dimethyl-1,4-phenylene oxide) (PPO), polyvinyl alcohol (PVA) and polyvinylchloride (PVC), are considered promising low-cost alternative materials.[30]

In 2013, one group from the Netherlands investigated the bulk membrane properties of cation-exchanging tailor-made membranes for RED using a non-fluorinated thermoplastic polymer known as sulfonated polyetheretherketone (SPEEK).[31] This study also prepared anion-exchanging polyepichlorohydrin (PECH) AEMs by a solvent evaporation method. Sulfonated SPEEK (65% and 40% sulfonation degree) CEMs were dissolved in 10 and 20 wt% N-methyl-2-pyrrolidon (NMP), cast with average thickness of 70 µm for SPEEK65 membranes and 55 µm for SPEEK40 membranes, and dried. The PECH AEMs and SPEEK CEMs were characterized and shown to have excellent electrochemical properties. When tested in a complete RED stack, the tailor-made

membranes exhibited higher gross power density (1.3 W/m^2) than RED stacks made with commercially available membranes. This work provides evidence that alternative polymer materials producing membranes with low resistance can contribute significantly towards optimizing power density of RED membrane stacks.

Another property that is particularly important for RED membranes in natural waters is high selectivity for monovalent ions.[32] Guler et al. (2014) was the first to test commercial AEMs with a negatively-charged coating on both sides to improve selectivity for monovalent ions for RED application.[33] The contents of the coating layer included 2-acryloylamido-2-methylprpanesulfonic acid (AMPS) as polyanion with sulfonic groups and N,N-methylenebis(acrylamide) (MBA) as the crosslinking agent. An in-situ synthesis method was used to prepare the membranes' reactive polymeric coating layer via UV irradiation on the membrane surface. This method preserved the bulk membrane structure, improved antifouling properties like hydrophilicity, and increased monovalent ion selectivity. The coated standard-grade commercial membrane performed similarly to commercially available monovalent-selective membranes in calculations of monovalent selectivity by bulk transport numbers, current-voltage, and limiting current density. Measurements from an RED stack test using thick coated membranes (~110 μm and above) did not yield significantly higher gross power densities than those of commercially available monovalent-selective membranes. Further research is needed with thinner membranes for a more significant improvement in power density.

A composite structure formed by introducing inorganic nanomaterial into an organic polymer matrix is another promising way to improve RED performance. The concept of combining organic polymer and inorganic nanoparticles to form composite

membranes has gained much interest owing to the ability to retain the desired properties from both components. The aim of incorporating inorganic filler materials into polymer-based materials is to enhance mechanical, chemical, and thermal stability of the polymer matrix. Fortunately, this blending can provide extra ion exchange functional groups to the membrane, which helps provide more ion migration, and thus allows improved conductivity as a single molecular composite.[18, 21b] Although formation of nanocomposites has been well studied, particularly for fuel cell and water purification applications,[21, 34] only a few studies have been reported in salinity gradient energy application, such as RED.[18] Nanocomposite IEMs allow extra ion exchangeable functional groups into the structure, which is advantageous to enhance the electrochemical characteristics of the membrane. Table 1 demonstrates the many membrane studies that have focused on combining and deriving the unique features of various inorganic nanoparticles with those of organic materials, predominantly in electrodialysis, fuel cell, and water treatment applications.

Organic–inorganic hybrid ion exchange membranes using PPO as the polymer backbone have been well-studied in applications outside of RED due to the enhanced thermal stability and mechanical strength. In one report, SiO_2 was blended into PPO through a sol–gel process of polymer precursors PPO–Si $(OCH_3)_3$ using tetraethoxysilane (TEOS) as the silicon source.[35] In addition to higher swelling-resistant properties, this hybrid membrane was found to have enhanced hydroxyl (OH^-) conductivity, which is particularly useful for alkaline fuel cells. In fact, the hydroxyl ion (OH^-) conductivity values were comparable to previously reported fluoropolymer-containing membranes (0.012-0.035 S cm^{-1} in the temperature range 30–90 °C). Additionally, with heat

treatment of between 120-140 °C during its preparation, the membranes' physicochemical properties (i.e., ion exchange capacity, hydrophilicity, OH^- conductivity, tensile strength) could be easily controlled by adjusting the heating temperature and time.

This year, the first report of nanocomposite CEMs applied in an RED stack for power generation was published.[18] In this study, various concentration loadings of functionalized iron (III) oxide (Fe_2O_3-SO_4^{2-}) particles were introduced into a sulfonated poly (2,6-dimethyl-1,4-phenylene oxide) (sPPO) polymer matrix. As the loading of Fe_2O_3-SO_4^{2-} increased, the electrochemical properties of the membranes improved. This enhancement was optimized in the range of 0.5-0.7 wt%. The membrane containing 0.7 wt% Fe_2O_3-SO_4^{2-} exhibited relatively higher permselectivity (87.65%) and lower area resistance (0.87 Ω cm^2). When tested in the RED stack, the highest gross power density obtained was 1.3 W/m^2, which exceeds the power output of the commercially available CSO (Selemion^{TM}, Japan) membrane. This new design of nanocomposite membrane showed promise as a feasible way to modify IEMs for a RED power generation process and was a major influence for this thesis work.

Table 1.1 Existing organic-inorganic nanocomposite membranes of various applications

Inorganic material	Organic material	Applications	References
Al_2O_3	PVA	Quaternized composite membrane for alkaline DMFC	(Yang et al., 2010)[36]
CeO_2	Nafion	Chemically durable proton exchange membrane for fuel cell	(Wang et al., 2012)[37]
$Cu_3(PO_4)_2$ $Ni_3(PO_4)_2$	PVC	Electrochemical evaluation of two composite IEMs	(Arsalan et al., 2013)[38]
Fe_2O_3	Nafion	High proton conductivity composite membrane for DMFC	(Sun et al., 2010)[14a]
Fe_2O_3	PPO	Salinity gradient power generation using RED	(Hong and Chen, 2014)[18]
Fe_2NiO_4	PVC	Performance evaluation of heterogeneous CEM	(Hosseini et al., 2012)[39]
MWNT	PVA	Crosslinked nanocomposite membrane for DMFC	(Yun et al., 2011)[40]
SiO_2	PPO	AEM for alkaline fuel cells: Effect of heat treatment	(Wu et al., 2009)[41]
SiO_2	PVA	Electrochemical characterization of AEM	(Nagarale et al., 2005)[42]
SiO_2	PPO	Fuel cell application	(Jeong et al., 2007)[43]
SiO_2	PVA	Thermally stable CEMs for fuel cell and chloro-alkali application	(Nagarale et al., 2004)[44]

Table 1.1 Continued

SiO_2	PVA	PEM for DMFC application	(Tripathi and Shahi, 2011)[45]
SiO_2	PVA/PPO	Double organic phases for diffusion dialysis (alkali recovery)	(Wu et al., 2012)[46]
SiO_2	PVDF	Electrochemical characterization of CEM	(Zuo et al., 2009)[47]
SiO_2	Nafion	Proton conducting membrane for DMFC	(Wang et al., 2011)[48]
SiO_2	Nafion	Investigation of composite membrane for PEMFC	(Ke et al., 2011)[49]
SiO_2	PES	Electrodialysis IEM for desalination	(Klaysom et al., 2010)[34a]
SiO_2	PPEK	Proton exchange membrane for DMFC	(Su et al., 2007)[13b]
SiO_2	PAES	Fuel cell application	(Lee et al., 2007)[13a]
SiO_2	PS	Performance evaluation: Proton and methanol transport	(Kim et al., 2006)[50]
SiH_4	PEO	Thermally stable negatively charged NF membrane	(Wu et al., 2005)[51]
TiO_2	PES	UV-irradiated TiO_2 for modification of UF membrane	(Rahimpour et al., 2008)[52]
TiO_2	PES	Performance evaluation of PES composite membrane	(Li et al., 2009)[53]
TiO_2	Nafion	Solid superacid composite membrane for DMFC	(Wu et al., 2008)[54]
TiO_2	Nafion	Electrochemical performance for DMFC	(Baglio et al., 2005)[55]
TiO_2	PVA	Pervaporation separation of water-isopropanol mixture	(Sairam et al., 2006)[56]
TiO_2	PVDF	Anti-fouling performance and water treatment	(Li et al., 2013)[57]
TiO_2	PES/PVA	Flux and salt rejection of NF membrane	(Pourjafar et al., 2012)[58]
TiO_2	PES	Fouling resistance of UF membrane	(Rahimpour et al., 2008)[52]
ZrO_2	Nafion	Asymmetric hybrid membrane for gas permeability	(Apichatachutapan et al., 1996)[59]
ZrO_2	Nafion	Conductive composite membrane for PEMFC	(Zhai et al., 2006)[60]
ZrO_2	Nafion	Solid polymer electrolyte electrolyzer application	(Siracusano et al., 2012)[61]
ZrO_2	PVDF	Performance evaluation of UF membrane	(Bottino et al., 2002)[62]
ZrO_2	Nafion	Performance at high temperature/low humidity for PEMFC	(Sacca et al., 2006)[63]
ZrO_2	Nafion	Proton conductivity for high temperature DMFC	(Navarra et al., 2009)[64]

PPO: Poly (2,6-dimethyl-1,4-phenylene oxide); PVA: Polyvinyl alcohol; PVDF: Polyvinylidene fluoride; PVC: Polyvinyl chloride; PES: Polyethersulfone; PPEK: Poly (phthalazinone ether ketone); PAES: Poly(arylene ether sulfone); PS: Polystyrene; PEO: Polyethylene oxide; MWNT: Multi-walled carbon nanotube; PEM: Polymer electrolyte membrane; PEMFC: Proton exchange membrane fuel cell; DMFC: Direct methanol fuel cell; NF: Nanofiltration; UF: Ultrafiltration.

Alterations to RED membrane stack design in conjunction with specialized membranes have shown improved performance in literature as well. One such study eliminated non-conductive spacers typically used in IEM stacks.[65] Two types of commercial heterogeneous membranes (Ralex CMH and AMH) were used because of their low melting temperatures. The dry membranes were thermally pressed between two aluminum molds. Once cooled, the pressed membranes were immersed in demineralized water then immersed in NaCl solution. By stacking the hot-pressed IEMs, a ridged profiled membrane was created that allowed feed water to flow freely through these channels. This method lowered the ohmic resistance of the stack and increased the boundary layer resistance compared to a conventional RED stack with non-conductive spacers.

CHAPTER 2

EXPERIMENTAL APPROACH

2.1 Materials

2.1.1 Selection of Polymer

Poly (2,6-dimethyl-1,4-phenylene oxide) (PPO) (Aldrich, analytical standard), was used for the polymer membrane. PPO was chosen due to its good mechanical, thermal, and chemical stability, especially when integrated with inorganic filler particles.[15] In addition to it is low cost, PPO has high film-forming properties, low-moisture uptake, and high glass transition temperature.[66] The structure of PPO consists of an aromatic ring, two methyl groups, and a phenol group (Figure 2.1). Various structural modifications, such as the functionalization of the benzene rings, methyl groups, and hydroxyl groups of PPO chains through electrophilic or radical substitutions, capping, and coupling, are possible due to the simple structure of PPO. The excellent electrochemical characteristics of sulfonated PPO (sPPO) have contributed to its wide use for various industrial applications.[67]

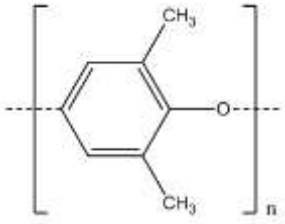

Figure 2.1 Molecular structure of poly (2,6-dimethyl-1,4-phenylene oxide)

Other polymer materials such as PVA and PVC were considered but ultimately ruled out due to poor conductivity and poor heat stability, respectively.

2.1.2 Selection of Inorganic Filler Particles

Silica (SiO_2) has been widely used as an ion exchangeable inorganic filler material for the synthesis of composite membranes, mostly for fuel cell and desalination applications.[13] Silica can take on an important role as a charge carrier in the composite membrane by modification of its particle surface. The surface of SiO_2 nanoparticle can be modified with $–SO_3H$ groups via a sulfonation reaction, which makes the material more hydrophilic with water molecules and functional in transporting ionic charges. Studies have reported that its versatility due to wide porosities and functionalities allows improved conductivity, water uptake, and mechanical stability of the membranes.[21] Two silicon dioxide (SiO_2, silica) nanopowders were used as the inorganic filler particles: 15 nm SiO_2 (US Research Nanomaterials, 99.5%) and 70 nm (US Research Nanomaterials, 98%).

2.1.3 Other Materials

Chloroform (Aldrich, anhydrous, 99%) was used as the organic solvent for PPO due to its low reactivity, miscibility with organics, and volatility (beneficial for our solvent evaporation technique). Chlorosulfonic acid (Aldrich, 99%) and sulfuric acid (Aldrich, 98%) were used in sulfonation of the polymer material and the inorganic filler particles, respectively. Both are hygroscopic and hazardous strong acids but they are very suitable in sulfonation. Methanol (Aldrich, anhydrous, 99.8%), used as a solvent, was mostly

evaporated off during drying of the sPPO. Dimethylsulfoxide (DMSO) (ACS grade, 99.9%) was obtained from VWR. DMSO is used in dissolution of the sPPO to prepare the membrane casting solution.

2.2 Material Preparation

2.2.1 Sulfonation of PPO

First, the appropriate amount of PPO was added to the chloroform solvent and stirred vigorously to yield a 6 wt% solution at room temperature. This solution was left stirring until the PPO was fully dissolved in the chloroform. The PPO-chloroform solution was gradually sulfonated with an 8 wt% chlorosulfonic acid and chloroform solution. The chlorosulfonic acid-chloroform solution was added dropwise to the PPO-chloroform solution over a time period of 30 minutes with vigorous stirring at room temperature. During this process, the sulfonated PPO (sPPO) started to precipitate out of solution, as evidenced by small brownish particles swirling in solution. After the sPPO was fully precipitated, it was washed with deionized (DI) water several times until the pH was between 5 and 6. After washing, the sPPO had an orange-white color and the texture was spongy. The sPPO was then dissolved in methanol over light heating (50 °C) for about an hour. The milky solution was poured into a Pyrex glass tray to form a thin film of about 1 mm thickness. This thin film was allowed to air-dry overnight at room temperature under the fume hood. After 24 hours, the dry sPPO was washed with DI water. Again, it was left to dry overnight. Finally, the dry sPPO was cut into small pieces

in order to make dissolution easier. The final sPPO product had a slight orange color and was mildly flexible.

2.2.2 Sulfonation of Silica Nanoparticles

The silica nanopowder was sulfonated with concentrated sulfuric acid (98%). The appropriate amount of SiO_2 was dissolved in 0.25 M H_2SO_4 solution. The particles were allowed to soak in the acid for 24 hours. The sulfonated SiO_2 was subsequently filtered and dried at 80 °C in a vacuum oven to remove any residual liquid. Last, to ensure the particles were completely dried, they were calcinated at 500 °C for 3 h to obtain a white sulfonated SiO_2 powder. This process was performed with both the 15 nm silica nanopowder and the 70 nm silica nanopowder.

2.3 Membrane Synthesis

The nanocomposite cation exchange membranes were then synthesized with the prepared sulfonated PPO polymer and sulfonated filler particles. A solvent evaporation method was employed to prepare the membranes. DMSO was used to dissolve the sPPO in preparation of the casting solution. 25 wt% solutions of sPPO in DMSO were prepared. When the sPPO was dissolved, 0-1 wt% of sulfonated SiO_2 was mixed with the polymer solution at 60 °C for 24 hours. This casting solution was left stirring overnight to properly disperse the particles. The resulting mixture was then cast onto glass plates with a doctor blade to obtain membranes with 30 µm thicknesses. To remove residual solvents, the membranes were dried in a vacuum oven for 24 h at 60 °C then for another 24 hours at 80 °C. The dried membranes were treated in 50 °C warm water for 15

minutes to remove them from the glass and cool them down. Then they were transferred to a 1 M HCl solution for 24 hours. The final membranes were rinsed with DI water and stored in 0.5 M NaCl solution until testing. These steps were performed to produce multiple membranes for each loading amount of silica nanoparticles (0 wt%, 0.2 wt%, 0.5 wt%, 0.8 wt%, 1 wt%,) and for each size silica nanoparticles. The thickness of the membranes was kept constant at 30 μm for consistency.

2.4 Membrane Characterization

2.4.1 Fourier Transform Infrared (FTIR) Spectroscopy

To investigate the chemical structures of the silica nanocomposite membranes, FTIR spectroscopy was used. FTIR spectra of sulfonated SiO_2 and PPO membranes were acquired with an FTIR spectrometer (Spectrum 400, PerkinElmer). This spectrometer collected 50 scans per sample at a resolution of 4 cm^{-1} and a spectral range of 4000-600 cm^{-1}. Background FTIR was the ambient air spectrum.

2.4.2 Morphology and Structure

The morphology of the inorganic filler particles was investigated by transmission electron microscopy (TEM, JEOL 100CX II). The structure of the surface and cross section of the prepared membranes was examined using scanning electron microscopy (SEM, Zeiss Ultra60 FE-SEM). To obtain a sharp cross-section for SEM, the samples were fractured after first being prepared in liquid nitrogen. Membrane samples were then dried overnight to preserve their structure.

2.4.3 Swelling Degree (SD)

SD is the extent to which the polymer membrane absorbs moisture. SD is important in determining the mechanical strength and stability of the membrane, as well as being influential in the ability of the membrane to be ion-selective and electrically resistant. It is measured as a percentage of water content per unit weight of dry membrane. To measure SD, a sample was taken from each membrane and immersed in DI water for at least 24 hours. Then, after removing the surface water from the sample, the weight of the swollen membrane was measured. Then, the same sample was air-dried overnight and weighed again to get the dry membrane mass. The SD of each membrane was calculated in weight percent by the following equation:

$$SD = \frac{W_{wet} - W_{dry}}{W_{dry}} \times 100\% \quad (1)$$

where W_{wet} and W_{dry} are the weight of the wet and the dry membrane, respectively. This method was adapted from previous work.[18]

2.4.4 Ion Exchange Capacity (IEC)

IEC was determined by using a titration method.[26] The membrane samples were first immersed in 1 M HCl for at least 15 hours. Then, the samples were rinsed with DI water to rid them of chloride ions. After rinsing, they were equilibrated in 1 M NaCl solution for at least six hours. The resulting solution, with displaced hydrogen ions from the membrane, was titrated with 0.01 M NaOH solution using phenolphthalein as an indicator. The IEC of membranes were then calculated by using the following equation:

$$IEC = \frac{C_{NaOH} \times V_{NaOH}}{W_{dry}} \quad (2)$$

where C_{NaOH} is the concentration of NaOH solution, V_{NaOH} is the volume of NaOH solution used and W_{dry} is the dry weight of the membrane. The IEC determination followed a previously described procedure.[18]

2.4.5 Charge Density

Charge density (CD, C_{fix}) is the measure of fixed number charged groups in the polymer backbone of the ion exchange membranes. This fixed charge density is expressed in units of milliequivalent of fixed groups per volume of water in the membrane (meq L^{-1}). The counter ion transport and ion permselectivity through the membrane is determined by the charge density. The calculation to determine the charge density is simply the IEC divided by the SD of the membrane, as seen in equation (3):

$$C_{fix} = \frac{IEC}{SD} \quad (3)$$

2.4.6 Resistance

A low membrane electrical resistance, or ability of the membrane to oppose the passage of electrical current, is most desirable for our application. Electrical resistance was measured in a two-compartment cell using 0.5 M NaCl aqueous solutions. The two electrodes were made of titanium and coated with Ru-Ir mixed metal oxides (Jing Run Beijing Science and Technology Research Institute Company, China). The resistance of the membranes was measured at room temperature by impedance spectroscopy (IS) using a Vertex Potentiostat/Galvanostat (Ivium Technologies, The Netherlands) in a frequency

range from 10-10^5 Hz with an oscillating voltage of 0.1 V amplitude.[68] The membrane resistance (R_{mem}) was determined by subtracting the resistance measured in the blank test (R_{sol}) from the resistance measured with the membrane under investigation (R_{cell}). This formula is based on the total cell resistance composition (i.e., $R_{cell}=R_{sol}+R_{mem}$).

2.4.7 Permselectivity

Permselectivity is the ability of the membrane to select for one species over another. A static membrane potential measurement was used to find the apparent permselectivity of each IEM. For this experiment, a two-compartment cell was separated by a membrane sample with an effective area of 4.8 cm^2. One compartment was filled with an aqueous solutions of 0.1 M NaCl and the other compartment was filled with an aqueous solution of 0.5 M NaCl. These two solutions could come in contact with the test membrane through a small hole in the center of the compartment. Two Ag/AgCl reference electrodes were used to measure the potential difference over the membrane and recorded the potential in a multimeter (Tektronix, USA). The permselectivity is calculated by dividing the measured membrane potential ($\Delta V_{measured}$) by the theoretical membrane potential ($\Delta V_{theoretical}$) as shown below:

$$\alpha(\%) = \frac{\Delta V_{measured}}{\Delta V_{theoretical}} \times 100 \quad (4)$$

where α is the membrane permselectivity (%). Note that the theoretical membrane potential is the membrane potential for an ideal 100% permselective membrane, which is estimated to be 0.0379 V from the Nernst equation.[69]

2.5 Membrane RED Power Performance

The sPPO-SiO_2 nanocomposite membranes were evaluated for power performance in an RED stack. As shown in Figure 2.2, RED setup has three cell pairs of alternately stacked AEMs (FAS) and CEMs (FKS) (Fumatech, Germany), between two titanium mesh end electrodes coated with iridium plasma. In addition, a CEM was placed at end of the stack as a shielding membrane. A measurement with this FKS membrane was made for comparison before being replaced with the synthesized nanocomposite membranes for testing. Electrode rinse solution was made with 0.25 M NaCl, 0.05 M $K_4Fe(CN)_6$, and 0.05 M $K_3Fe(CN)_6$ and pumped through the electrode compartments at a flow rate of 300 ml min^{-1}. The artificial feed water simulating seawater was 0.5 M NaCl and simulating river water was 0.017 NaCl, held in 5L batch containers (McMaster-Carr, USA). This synthetic sea and river water was passed though the water compartments formed by woven fabric spacers (thickness: 250 µm, porosity 60%) (Figures 2.4 and 2.5). Masterflex peristaltic pumps (Cole-Parmer, USA) circulated the saline and dilute feed water and the electrode rinsing solution through the RED stack at various flow rates.

The power performance was measured with an external Vertex Potentiostat (Ivium Technologies, The Netherlands) in galvanostatic mode. Once the voltage and electrical current were measured with the potentiostat, the gross power density was estimated and then corrected by subtracting the power generated in a blank test with only a single AEM in the stack.

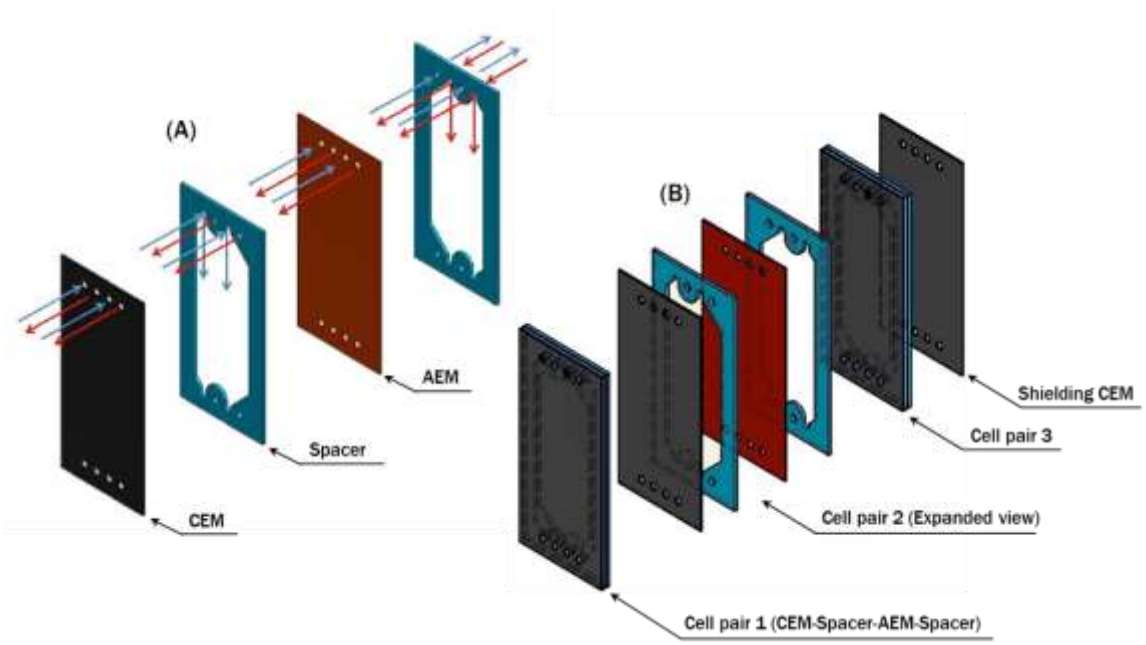

Figure 2.2 Visualization of the membrane configuration in a RED stack used in this performance test: (A) flow schematic for a single RED cell, and (B) Membrane stack consisting of three repeating cell pairs. Note that the red and blue arrows in (A) represent two different feed streams (saline water or fresh water).

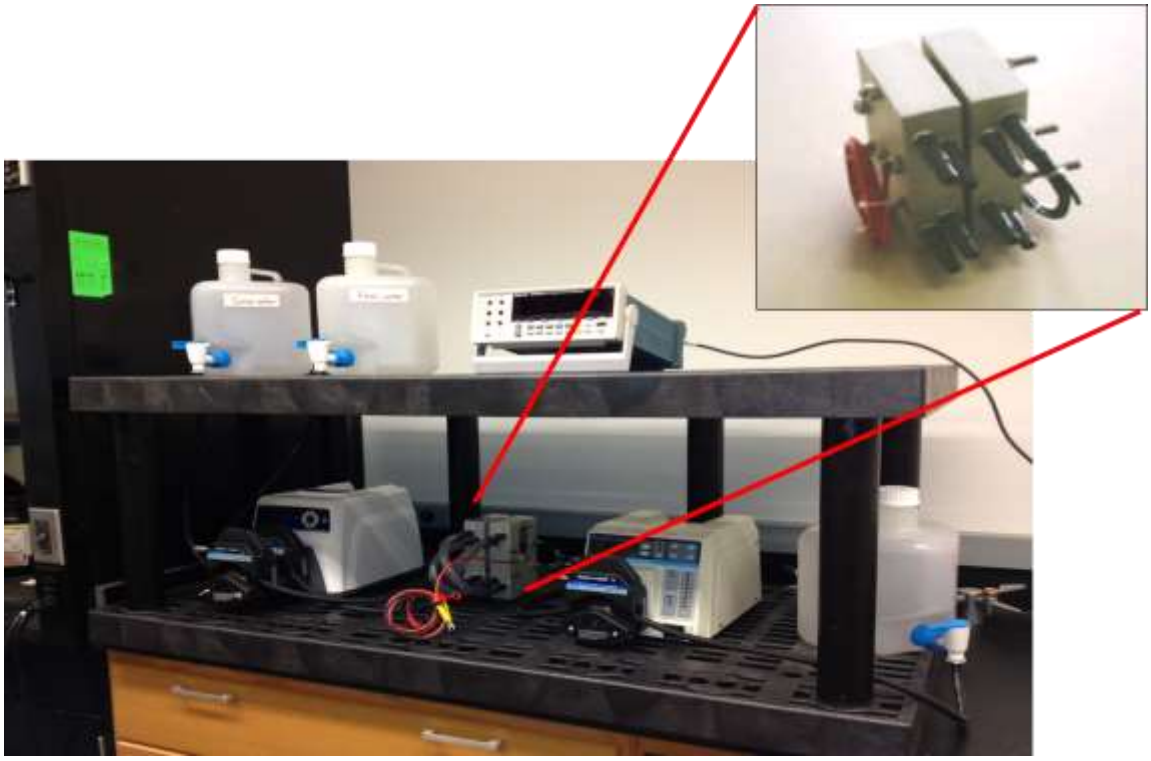

Figure 2.3 RED stack setup in Daniel Laboratory. Solution reservoirs and digital multimeter (top), saline and dilute pump (bottom left), membrane module (bottom middle), and electrode rinse pump (bottom right).

Figure 2.4 Spacers from RED stack

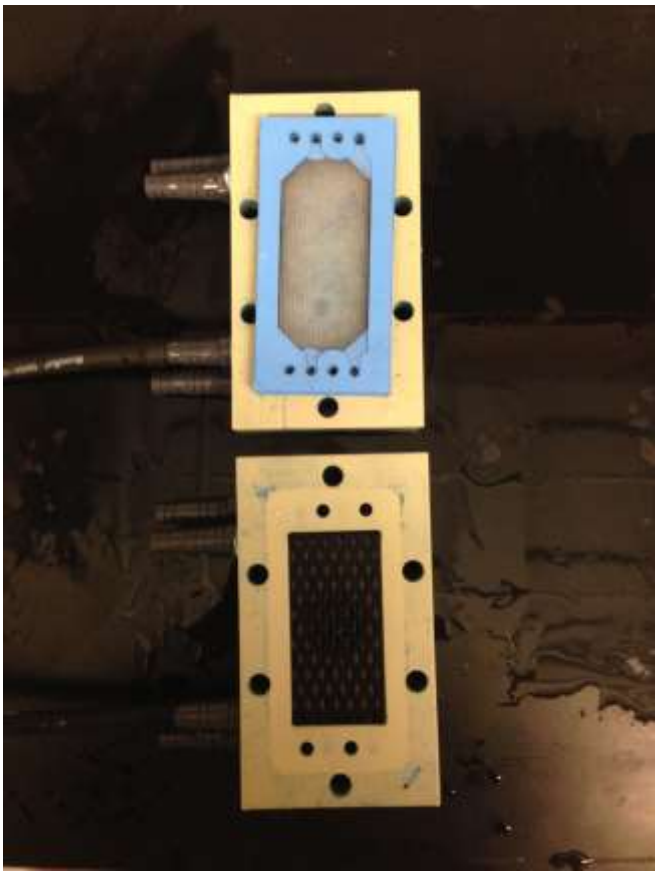

Figure 2.5 Interior view of the RED stack

CHAPTER 3

RESULTS AND DISCUSSION

3.1 FTIR Spectra Study

Figure 3.1 shows the FTIR spectra of silica composite membrane samples. As shown in the figure, the original PPO polymer spectra (a) displayed a C-H stretch of CH_2 and CH_3 between 2868 and 2970 cm^{-1} and a C-O-C stretch at 942 cm^{-1}. These peaks were mimicked in each of the spectrum lines for the various silica loadings in the nanocomposite membranes (b-e). In all spectra (a-f), there were characteristic absorption peaks at 1060 cm^{-1}, which indicated the presence of the $–SO_3H$ group, which was substituted onto the PPO aromatic rings during the sulfonation reaction. All the spectra of sPPO membranes (a-e) showed a large band in the range of 3300 and 3500 cm^{-1}. This large band can be attributed to the hydrogen reaction between –OH groups and $–SO_3H$. At 1172 cm^{-1}, the symmetric stretching vibration bands, which are characteristic of O=Si=O in the SO_3H groups, were observed (b-f). These FTIR results demonstrated the successful functionalization of the PPO and SiO_2 nanoparticles with SO_3H groups during the sulfonation process. Also, the presence of ion exchangeable groups in these organic and inorganic components was evident in the results.

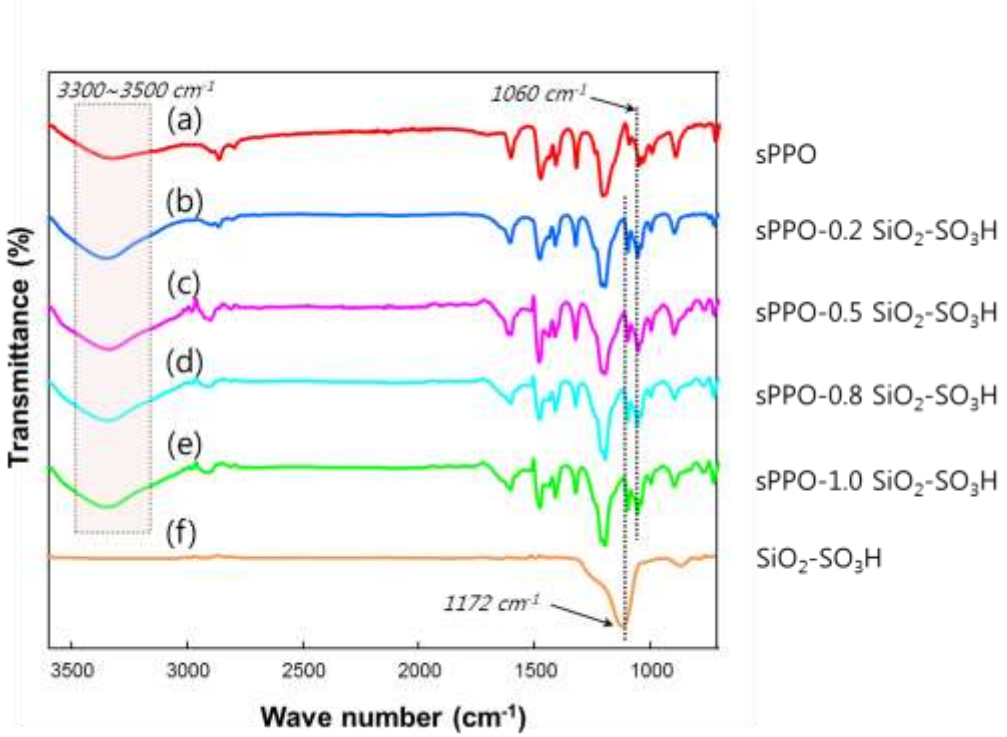

Figure 3.1 FTIR spectra of nanocomposite membranes: (A) Pure sPPO, (B) 0.2 wt% SiO_2-SO_3H, (C) 0.5 wt% SiO_2-SO_3H, (D) 0.8 wt% SiO_2-SO_3H, (E) 1.0 wt% SiO_2-SO_3H, (F) SiO_2-SO_3H.

3.2 Morphology of Inorganic Filler Particles and Membranes

The silica particles of two different sizes were sulfonated according to previously reported procedure.[48] Figure 3.2 displays the TEM images of the 15 nm and 70 nm sulfonated SiO_2 nanoparticles. The nanoparticles were added to sulfuric acid solution then mixed with the sPPO polymer solution to form nanocomposite membranes by using the blending method first and then followed by the phase inversion technique. The surface and cross-sectional morphologies of the prepared membranes were observed from SEM, as seen in Figure 3.3. As inorganic loading increased (getting closer to 1.0 wt%), a higher membrane porosity and relatively larger-sized pores was observed, especially for the membranes containing bigger filler particles (70 nm). The increase in pore formation is attributed to the low polymer-particle adhesion at their interfacial zone. The result is

the creation of more voids with additional porosity in the matrix. Relatively larger pores and higher porosity for the membranes with the bigger filler particle may also arise because of poor interaction between polymer and particle (i.e., larger interfacial gaps) compared with those membranes with smaller sized particles (15 nm). The energy-dispersive X-ray spectroscopy (EDS) mapping technique was utilized to elucidate the distribution and aggregation of filler particles in the membranes. Figure 3.4 shows the dispersion of silicon throughout a sample of the sPPO nanocomposite membrane. In the figure, the filler particles are well-dispersed throughout the polymer matrix with some signs of particle agglomeration, which is a possible cause of the visible pores formed in the structure.

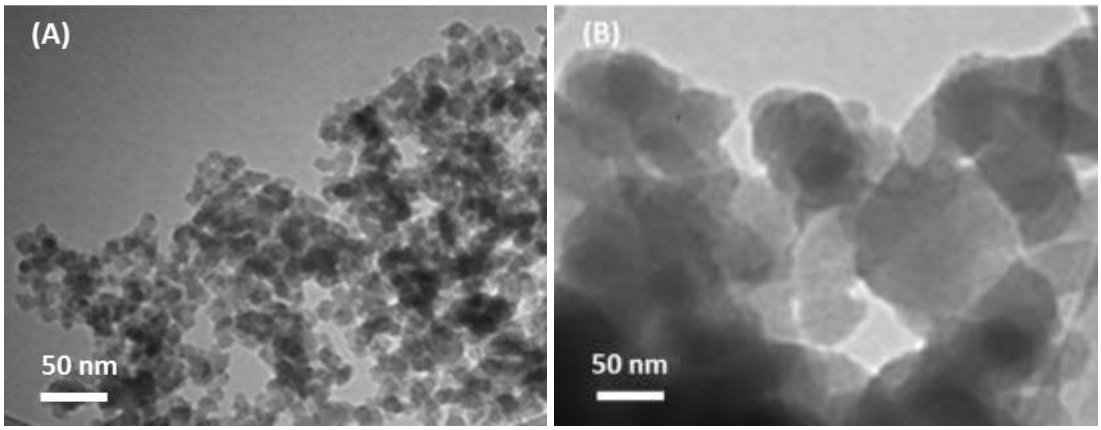

Figure 3.2 TEM images of sulfonated SiO_2 nanoparticles with sizes of (A) 15 nm and (B) 70 nm.

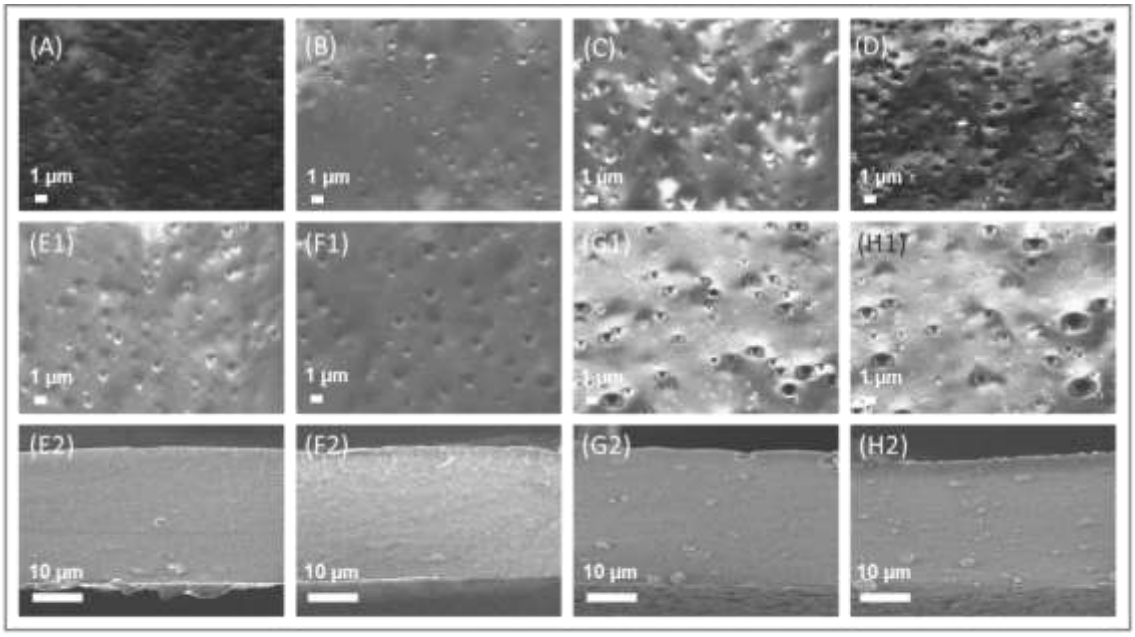

Figure 3.3 SEM micrographs of sPPO composite membranes: (A) 0.2 wt% SiO_2-SO_3H (15 nm), (B) 0.5 wt% SiO_2-SO_3H (15 nm), (C) 0.8 wt% SiO_2-SO_3H (15 nm), (D) 1.0 wt% SiO_2-SO_3H (15 nm), (E1, E2-H1, H2) 0.2, 0.5, 0.8, and 1.0 wt% SiO_2-SO_3H (70 nm), respectively.

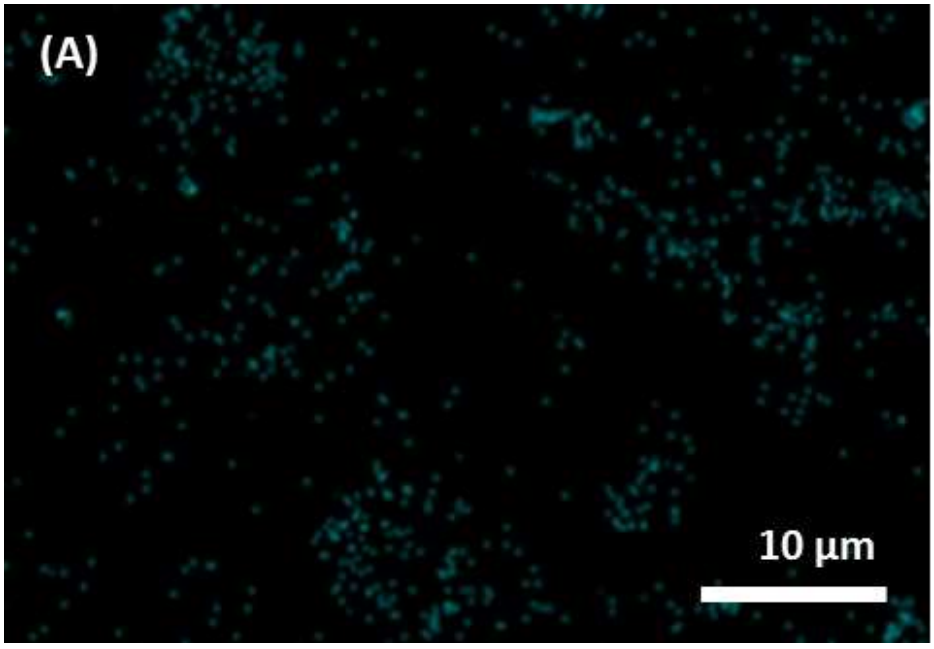

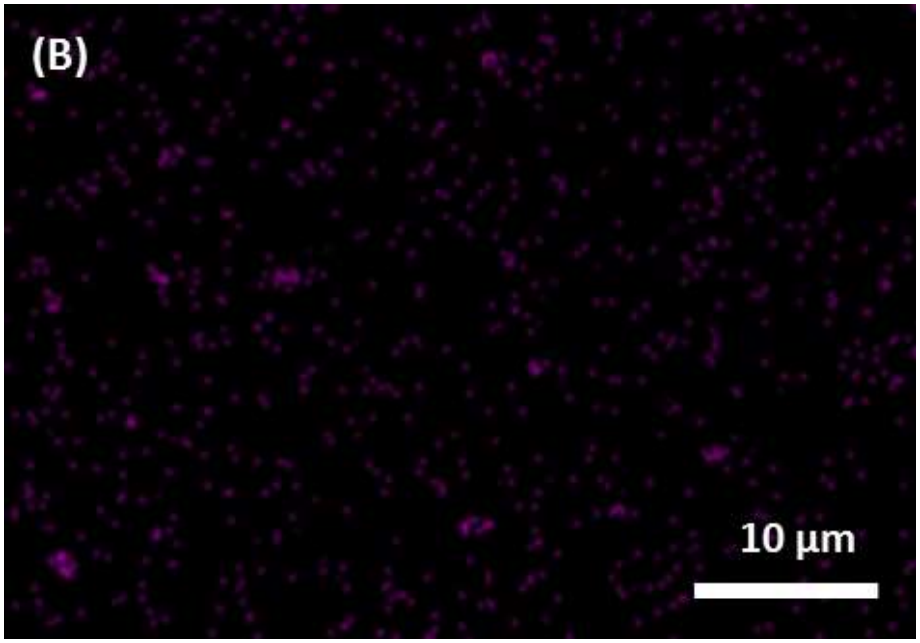

Figure 3.4 EDS-mapping analysis of sPPO composite membranes: (A) 0.2 wt% SiO_2-SO_3H (70 nm), and (B) 0.5 wt% SiO_2-SO_3H (70 nm). Note that cyan and pink dots represent the dispersion of silica nanoparticles on the surface of corresponding membranes.

3.3 Physicochemical Properties of Membranes

3.3.1 Swelling Degree

SD is typically proportional to IEC and inversely proportional to cross-linkage.[70] As IEC increases, membrane swelling generally increases; but other factors, such as ion exchange group species and polymer material, can cause SD to fluctuate. Higher SD can be indicative of low mechanical strength and stability of the membrane. From the data displayed in Figure 3.5, there is a trend of increasing SD with increasing silica nanoparticle size. This can be explained from a microscopic level. As seen in Figure 3.3, bigger nanoparticles allow for larger pores within the membrane. This increase in pore size allows more water molecules to be absorbed by the membrane. On the other hand,

the smaller nanoparticles with relatively small pores are less able to take up water molecules, leading to a lower SD.

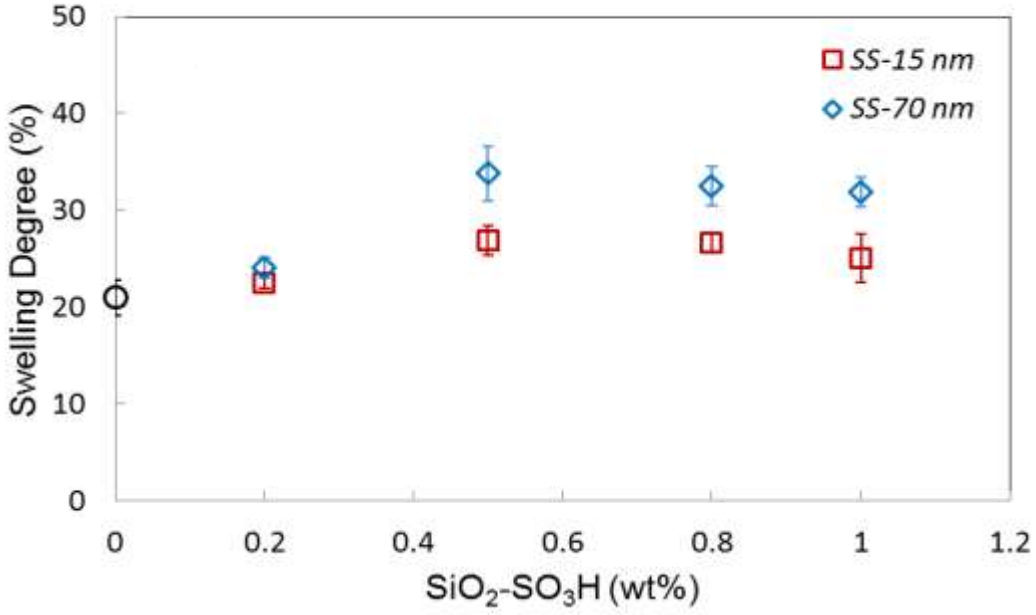

Figure 3.5 Swelling degree of sPPO nanocomposite membranes with different sizes of inorganic filler particles at various loading amount. Note that *SS* denotes the sulfonated SiO_2.

3.3.2 Ion Exchange Capacity

IEC is an important characteristic of ion exchange membranes for RED since it affects most of the other properties of the membrane.[12] For both sizes of silica nanoparticles, the trend found from analysis of our IEC results shows an increase until a peak at 0.5 wt% loading. After this peak, the IEC dramatically decreases when 0.8 wt% silica loading is applied then gradually decreases at 1.0 wt%. This can be explained by the fact that an increase in loading of sulfonated silica increases the functionalized groups within the membrane and allows for optimized exchange of ions. But increasing the loading too much can cause agglomeration of the nanoparticles, decreasing the ability of the membrane to productively exchange ions.

Central to this study is the effect of nanoparticle size on membrane performance. The nanocomposite membranes containing the bigger nanoparticles (70 nm) consistently performed better in IEC tests than those with the smaller nanoparticles. The difference is most apparent for the 0.5 wt% membrane, which could indicate that the loading is interconnected when considering nanoparticle size in relation to ability to exchange ionic species. The nanoparticle size is significant because as the size of the nanoparticle increases, the surface of ion accessible functionalized groups at interfacial (polymer and filler) zone increases, and, therefore, an increased ability to exchange ions. For this reason, the 70 nm-containing membranes exhibited better IEC in all loading percentages. But, there is a limit to this beneficial feature; as shown in Figure 3.6, there is a loss of accessible ion exchange groups at higher loading (0.8 ~ 1.0 wt%). The loss of accessible ion exchange groups at high loading is related to a reduction of the surface of charged groups. This reduction of the surface of charged groups is largely due to particle agglomeration and indicates poor interaction between the sulfonated silica nanoparticles and the polymer. On the other hand, at low silica loading (0.2 wt%), there is good interaction between the filler particles and the polymer.

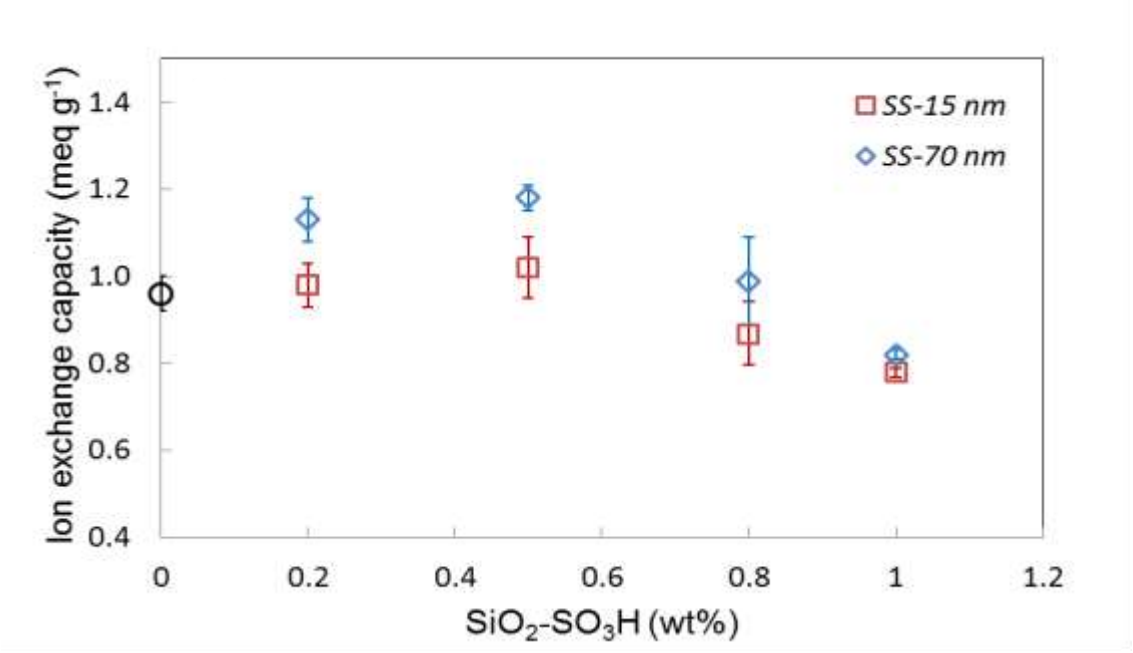

Figure 3.6 Ion exchange capacity of sPPO nanocomposite membranes with different sizes of inorganic filler particles at various loading amount. Note that *SS* denotes the sulfonated SiO_2.

3.4 Electrochemical Behavior of Membranes

The membrane properties of permselectivity and area resistance are related to the degree of IEC and SD of the membranes. Given that the fixed charge density is determined by the IEC over SD (Eq. 1), permselectivity and area resistance are often demonstrated by the fixed CD, or the number of charged functional groups (counter ions) in the membrane. High CD indicates a stronger co-ion exclusion. Permselectivity and resistance of the prepared membranes are presented as a function of charge density in Figure 3.7. There is a slight trend of increasing permselectivity with increasing CD, which is the result of effective co-ion exclusion, which facilitates the enhanced counter ion transport, leading higher permselectivity. Figure 3.7 displays results showing a more apparent correlation between CD and area resistance for the prepared nanocomposite

membranes. This semi-linear trend is often the case for the membranes with same structure and chemistry as well as a comparable degree of cross-linking.[31, 71]

The relationship between inorganic filler loading and permselectivity is demonstrated in Figure 3.8. The permselectivity of the prepared nanocomposite membranes increased with increasing sulfonated SiO_2 loading, peaking at 0.5 wt%. As more sulfonated silica nanoparticles were added to the membranes, the loss of the accessible functional groups in sulfonated silica is likely the cause of the decrease in permselectivity. The loss of accessible function groups causes low IEC and fixed charge density and results in poor selective ion transport of counter ions. Low resistance is generally expected with more ionic groups present in the matrix due to the greater swelling degree.[9, 18] The membranes containing 0.5 wt% SiO_2-SO_3H had the highest IEC and SD and had the lowest resistance.

As seen in Figures 3.8 and 3.9, nanoparticle size was of considerable influence on the degree of permselectivity and resistance. The effect of filler particle size on these ion transport properties may be associated with the structure and pore formation of the membranes, which often depends on the interaction between polymer and filler particle.[72] As previously discussed, nanoparticle size plays a key role in creating membrane porosity. The membranes containing bigger filler particles (70 nm) have larger pores or higher porosity, which lowers the ability to effectively select counter ionic species, leading lower permselectivity compared to the membranes containing smaller filler particles. On the other hand, the formation of such pore structure with the bigger filler particles also promotes enhanced migration of ionic species, which, in turn, resulted in relatively lower resistance at all filler loadings (Figure 3.9). The best IEC, SD, and

permselectivity were exhibited by the membranes loaded with 0.5 wt% SiO_2-SO_3H of the 70 nm particles. These also exhibited the lowest amount of resistance. As more SiO_2-SO_3H (both particle size) were incorporated, the resistance increased in a similar fashion. The reason for the increase in the resistance is the relatively low charge density of membranes at higher percentages of inorganic filler loading (0.8 and 1.0 wt%).

All measured membrane properties are displayed in Table 2. These values are averages from at least three replicate membrane property tests. As Table 2 shows, resistance (the most important membrane property to be minimized) is lower than the commercially available FKS membrane for all the prepared nanocomposite membranes.

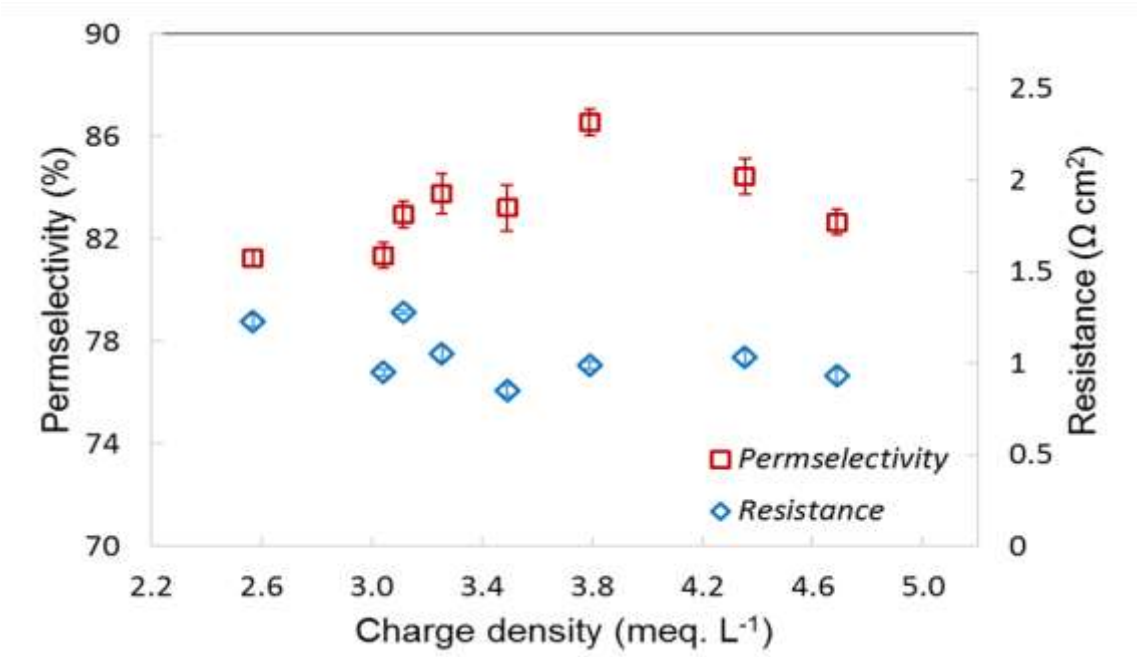

Figure 3.7 Membrane permselectivity and area resistance of sPPO nanocomposite membranes as a function of charge density

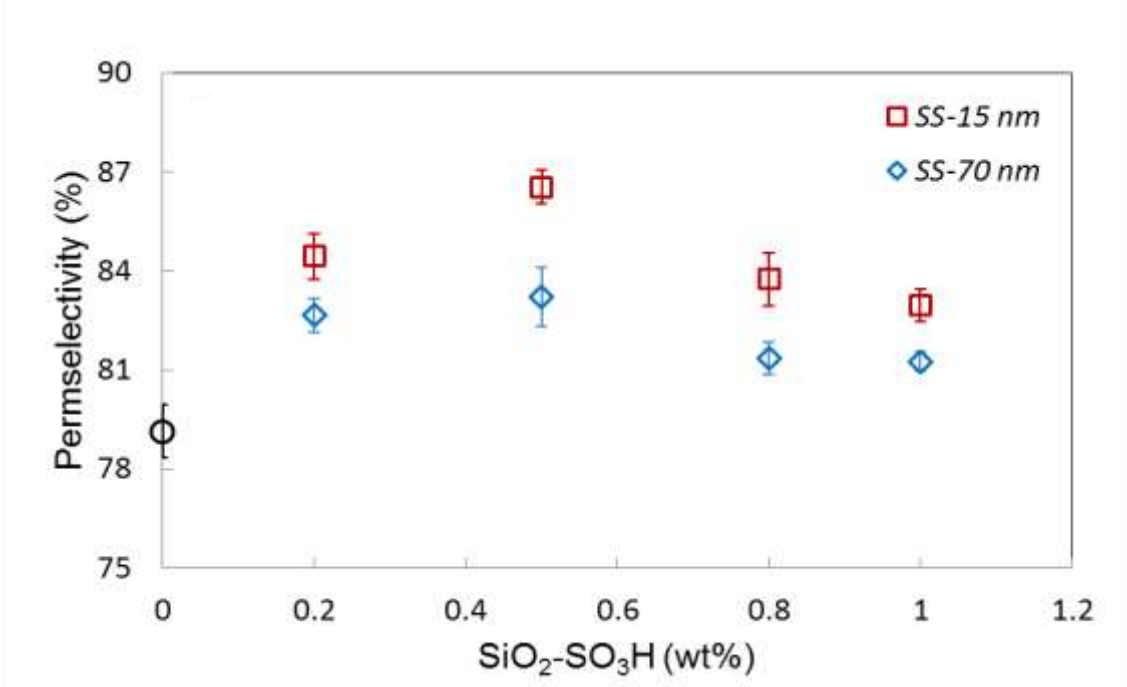

Figure 3.8 Membrane permselectivity of sPPO nanocomposite membranes of different size of inorganic filler particles at various loading amount. Note that *SS* denotes the sulfonated SiO_2.

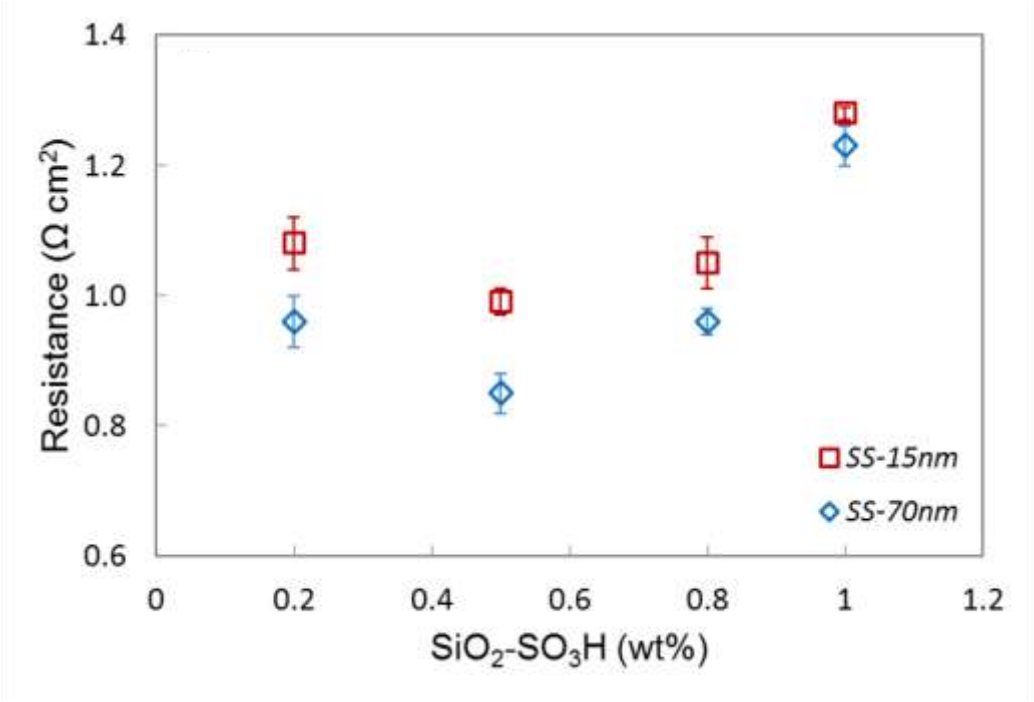

Figure 3.9 Membrane area resistance of sPPO nanocomposite membranes of different size of inorganic filler particles at various loading amount. Note that *SS* denotes the sulfonated SiO_2 and the resistance data for the pristine membrane (0 wt% SiO_2-SO_3H) lied outside the axis scale range.

Table 3.1 Physical and electrochemical properties of the prepared membranes

Membranes	IEC [meq. g^{-1}]	SD [%]	CD [meq. g H_2O^{-1}]	Permselectivity [%]	Area resistance [Ω cm^2]
0 SS	0.96	21	4.6	79.1	1.87
0.2 SS-15 nm	0.98	23	4.4	84.4	1.03
0.5 SS-15 nm	1.02	27	3.8	86.5	0.99
0.8 SS-15 nm	0.87	27	3.3	83.8	1.05
1.0 SS-15 nm	0.78	25	3.1	83.0	1.28
0.2 SS-70 nm	1.13	24	4.7	82.7	0.93
0.5 SS-70 nm	1.18	34	3.5	83.2	0.85
0.8 SS-70 nm	0.99	33	3.0	81.4	0.95
1.0 SS-70 nm	0.82	32	2.6	81.3	1.23
FKS[a]	1.49	15	9.9	94.0	1.49

IEC: ion exchange capacity; SD: swelling degree; CD: charge density; SS: sulfonated SiO_2.

[a] FKS is a commercial CEM from Fumatech, Germany with a thickness of 30 μm.

3.5 Power Density in RED

The power density is determined by the internal resistance of the entire RED stack and the Donnan electrical potential generated. These two features are influenced by other factors: internal resistance is determined by membrane resistance, spacer shadow effect, and solution resistance and the electrical potential is determined by membrane selectivity, salinity gradient, and concentration polarization.

We measured the gross power density of the CEMs, each containing different size nanoparticles at different inorganic loadings, and proceeded to compare the results with the gross power density of the commercial membrane (Fumatech FKS). Since the RED stack needs AEMs placed alternately with the CEMs, the Fumatech FAS membranes were used as reference AEMs in the RED stack for all tests.

Figure 3.10 shows the gross power density of the stack generated from the membranes as a function of the feed flow rates. Gross power density increases as the flow

rate of (rapidly renewed) feed waters increases. This is due to the increase in facilitation of ion transport because of reduced boundary layer resistance at the membrane surface. This low internal electrical resistance leads to high power density. The highest power density of 1.3 W m^{-2} was exhibited by the membrane with a blend ratio of 0.5 wt% SiO_2-SO_3H with a particle size of 70 nm at the highest feed flow rate. The membrane with the same blend ratio containing the smaller nanoparticles (15 nm) had a significantly lower power density (Figure 3.10). In our experiments, membranes containing bigger filler particles produced higher power densities. This observation is in agreement with Figure 3.9 that shows relatively lower area resistance with the 70 nm-containing membranes than with the 15 nm-containing membranes. The gross power density did not appear to be affected by the fact that the 15 nm-containing membranes exhibited a higher degree of permselectivity throughout the various inorganic loadings. Similarly, the commercial FKS membrane had a lower gross power density when compared with the membranes with lower permselectivity and lower area resistance. Due to these observations, we found that, regardless of high selectivity, the area resistance of the prepared membranes is the dominant characteristic and has the most influential impact on the overall RED power generation. In general, the effect of the size of inorganic filler particles on power performance of prepared nanocomposite CEMs was about a 10 % average difference at various loading concentrations, in favor of the 70 nm particles over the 15 nm particles. Since inorganic filler nanoparticle size impacts the final membrane structure and its electrochemical properties, size may be a key driver to achieving the optimal power density measurement from an RED stack.

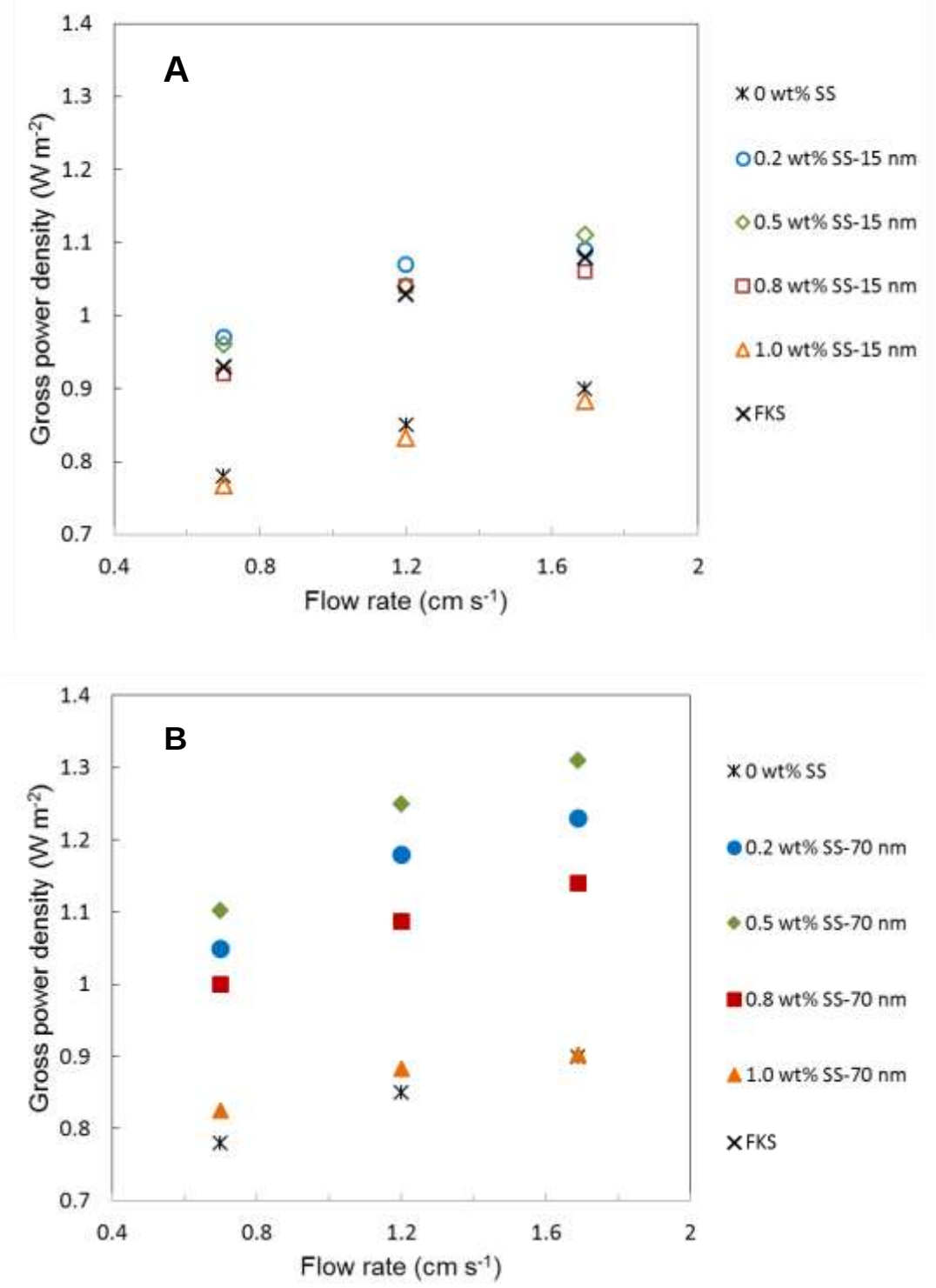

Figure 3.10 Gross power density as a function of flow rate for the prepared nanocomposite membranes with **(A)** 15 nm silica nanoparticles and (**B**) 70 nm silica nanoparticles at various loadings. The performance of the FKS membrane is shown for comparison on both figures.

CHAPTER 4

CONCLUSIONS AND FUTURE DIRECTION

4.1 Conclusions

The goal of this research was to prepare novel CEMs with two differently sized silica nanoparticles at a variety of loading amounts in order to compare the effects on membrane properties (physical and electrochemical) and final RED power density. The membranes were synthesized by a solvent evaporation method using sulfonated PPO blended with SiO_2-SO_3H particles. The methods used to make and test the membranes were adopted from various reliable publications. This investigation is the first of its kind to explore using different nanoparticle sizes in tailor-made composite membranes to improve RED performance.

As shown in the results, the higher the IEC and the lower the electrical resistance, the greater the RED power density. For all loadings, the 70 nm particle-containing membranes out-performed the corresponding 15 nm particle-containing membranes in terms of power density. This power density difference can be attributed to the measured lower electrical resistance of the nanocomposite membranes with the larger nanoparticles, which is the key factor in predicting the power output. Interestingly, though the permselectivity was higher for the prepared membranes with the smaller nanoparticles for all loadings (due to the smaller sized pores strengthening the effective co-ionic exclusion), the effect of this relatively higher ion selectivity was not relayed in the RED power measurements. This observation is indicative of the stronger correlation between low resistance and high RED power density.

The membrane with the most favorable physical and electrochemical characteristics overall had a loading of 0.5 wt% SiO_2-SO_3H. When this optimal loading of the membrane was exceeded, the inorganic filler particles began to aggregate, or form clusters. At the higher loadings, the clusters started to hinder the membrane properties, diminishing the membranes effectiveness for ion exchange applications.

The membranes containing the bigger filler particles exhibited approximately 9.3% lower resistance than those with the smaller filler particles, resulting in a 10% (average) higher gross power density for all loading concentrations. From our findings, more desirable electrochemical properties and greater RED power densities can be generated by incorporating optimized inorganic filler particles in optimized loading amounts into the polymer membrane structure.

4.2 Future Direction

The results presented here are encouraging and can serve as the basis of further investigations into nanocomposite membranes for RED applications. Future research could delve into other nanoparticle materials with lower cost, better conductivity, or better incorporation methods.

In addition to membrane improvements, the RED stack design is still under development. To reach a higher energy generation from the RED stack, spacers, electrode systems, cell dimensions, and fluid flow rates should be optimized. This research is ongoing and will hopefully be tested with real, natural water conditions to ensure minimal membrane fouling and maximum membrane environmental stability.

Optimizing RED systems is a promising way to combat greenhouse gas emissions from current fossil fuel use by providing a clean, sustainable source of energy.

REFERENCES

1. Agency, I. E. Key World Energy Statistics 2013, p. 80. (accessed October 22, 2014).
2. Santoyo-Castelazo, E.; Azapagic, A., Sustainability assessment of energy systems: integrating environmental, economic and social aspects. *J. Clean Prod.* **2014,** *80*, 119-138.
3. IPCC *Climate Change 2014: Imapcts, Adaptation, and Vulnerability*; Contribution of Working Group II to the Fifth Assessment Report of the Intergovernmental Panel on Climate Change [Field, C.B., V.R. Barros, D.J. Dokken, K.J. Mach, M.D. Mastrandrea, T.E. Bilir, M. Chatterjee, K.L. Ebi, Y.O. Estrada, R.C. Genova, B. Girma, E.S. Kissel, A.N. Levy, S. MacCracken, P.R. Mastrandrea, and L.L. White (eds.)]: Cambridge, United Kingdom and New York, NY, USA, 2014.
4. Hester, R. E.; Harrison, R. M., *Issues in Environmental Science and Technology: Carbon Capture : Sequestration and Storage*. Royal Society of Chemistry: Cambridge, UK, 2009; Vol. 29.
5. Wick, G. L.; Schmitt, W. R., Prospects for Renewable Energy from the Sea. *Marine Technology Society Journal* **1977,** *11* (5 & 6), 21.
6. Laboratory, N. R. E. *Renewable Electricity Futures Study*; NREL/TP-6A20-52409: Golden, CO, 2012.
7. Post, J. W.; Veerman, J.; Hamelers, H. V. M.; Euverink, G. J. W.; Metz, S. J.; Nymeijer, K.; Buisman, C. J. N., Salinity-gradient power: Evaluation of pressure-retarded osmosis and reverse electrodialysis. *Journal of Membrane Science* **2007,** *288* (1-2), 218-230.
8. Yip, N. Y.; Elimelech, M., Comparison of Energy Efficiency and Power Density in Pressure Retarded Osmosis and Reverse Electrodialysis. *Environmental Science & Technology* **2014,** *48* (18), 11002-11012.
9. Dlugolecki, P.; Nymeijer, K.; Metz, S.; Wessling, M., Current status of ion exchange membranes for power generation from salinity gradients. *Journal of Membrane Science* **2008,** *319* (1-2), 214-222.
10. Vermaas, D. A.; Guler, E.; Saakes, M.; Nijmeijer, K., Theoretical power density from salinity gradients using reverse electrodialysis. *Technoport 2012 - Sharing Possibilities and 2nd Renewable Energy Research Conference (Rerc2012)* **2012,** *20*, 170-184.
11. Vermaas, D. A.; Saakes, M.; Nijmeijer, K., Doubled power density from salinity gradients at reduced intermembrane distance. *Environmental Science and Technology* **2011,** *45* (16), 7089-7095.
12. Güler, E.; Elizen, R.; Vermaas, D. A.; Saakes, M.; Nijmeijer, K., Performance-determining membrane properties in reverse electrodialysis. *Journal of Membrane Science* **2013,** *446*, 266-276.
13. (a) Lee, C. H.; Min, K. A.; Park, H. B.; Hong, Y. T.; Jung, B. O.; Lee, Y. M., Sulfonated poly(arylene ether sulfone)-silica nanocomposite membrane for direct methanol fuel cell (DMFC). *J Membrane Sci* **2007,** *303* (1-2), 258-266; (b) Su, Y. H.; Liu, Y. L.; Sun, Y. M.; Lai, J. Y.; Wang, D. M.; Gao, Y.; Liu, B. J.; Guiver, M. D., Proton exchange membranes modified with sulfonated silica nanoparticles for direct methanol fuel cells. *J Membrane Sci* **2007,** *296* (1-2), 21-28; (c) Klaysom, C.; Marschall, R.; Moon, S. H.; Ladewig, B. P.; Lu, G. Q. M.; Wang, L. Z., Preparation of porous composite ion-exchange membranes for desalination application. *Journal of Materials Chemistry* **2011,** *21* (20), 7401-7409.
14. (a) Sun, L. L.; Wang, S. L.; Jin, W.; Hou, H. Y.; Jiang, L. H.; Sun, G. Q., Nano-sized Fe2O3-SO42- solid superacid composite Nafion (R) membranes for direct methanol fuel cells. *International Journal of Hydrogen Energy* **2010,** *35* (22), 12461-12468; (b) Colomer, M. T.;

Zenzinger, K., Mesoporous alpha-Fe2O3 membranes as proton conductors: Synthesis by microwave-assisted sol-gel route and effect of their textural characteristics on water uptake and proton conductivity. *Microporous and Mesoporous Materials* **2012,** *161*, 123-133; (c) Hasanabadi, N.; Ghaffarian, S. R.; Hasani-Sadrabadi, M. M., Magnetic field aligned nanocomposite proton exchange membranes based on sulfonated poly (ether sulfone) and Fe2O3 nanoparticles for direct methanol fuel cell application. *International Journal of Hydrogen Energy* **2011,** *36* (23), 15323-15332.

15. Xu, T., Ion exchange membranes: State of their development and perspective. *Journal of Membrane Science* **2005,** *263* (1–2), 1-29.

16. Klaysom, C.; Germain, L.; Burr, S.; Ladewig, B. P.; Wang, L. Z.; Da Costa, J. D.; Lu, G. Q. M., Preparation of new composite membranes for water desalination using electrodialysis. In *Smart Materials V*, Voelcker, N. H.; Thissen, H. W., Eds. 2008; Vol. 7267.

17. Klaysom, C.; Moon, S. H.; Ladewig, B. P.; Lu, G. Q. M.; Wang, L. Z., Preparation of porous ion-exchange membranes (IEMs) and their characterizations. *J Membrane Sci* **2011,** *371* (1-2), 37-44.

18. Hong, J. G.; Chen, Y., Nanocomposite reverse electrodialysis (RED) ion-exchange membranes for salinity gradient power generation. *J Membrane Sci* **2014,** *460*, 139-147.

19. Klaysom, C.; Moon, S.-H.; Ladewig, B. P.; Max Lu, G. Q.; Wang, L., The influence of inorganic filler size on composite ion exchnage membranes for desalination. *J. Phys. Chem* **2011,** *115*, 15124-15132.

20. (a) Colomer, M. T.; Zenzinger, K., Mesoporous alpha-Fe2O3 membranes as proton conductors: Synthesis by microwave-assisted sol-gel route and effect of their textural characteristics on water uptake and proton conductivity. *Microporous and Mesoporous Materials 161*, 123-133; (b) Gohil, G. S.; Binsu, V. V.; Shahi, V. K., Preparation and characterization of mono-valent ion selective polypyrrole composite ion-exchange membranes. *J Membrane Sci* **2006,** *280* (1-2), 210-218; (c) Gui, L.; Wang, H.; Shentu, B.; Weng, Z., Synthesis and characterization of low-molecular-weight poly(2,6-dimethyl-1,4-phenylene oxide) in water. *Journal of Applied Polymer Science* **2012,** *128* (5), 2919-2926.

21. (a) Gomes, D.; Marschall, R.; Nunes, S. P.; Wark, M., Development of polyoxadiazole nanocomposites for high temperature polymer electrolyte membrane fuel cells. *J Membrane Sci* **2008,** *322* (2), 406-415; (b) Wilhelm, M.; Jeske, M.; Marschall, R.; Cavalcanti, W. L.; Tölle, P.; Köhler, C.; Koch, D.; Frauenheim, T.; Grathwohl, G.; Caro, J.; Wark, M., New proton conducting hybrid membranes for HT-PEMFC systems based on polysiloxanes and SO3H-functionalized mesoporous Si-MCM-41 particles. *J Membrane Sci* **2008,** *316* (1–2), 164-175.

22. Nalwa, H. S., Handbook of organic-inorganic hybrid materials and nanocomposites. **2003**.

23. (a) Veerman, J.; Saakes, M.; Metz, S. J.; Harmsen, G. J., Electrical Power from Sea and River Water by Reverse Electrodialysis: A First Step from the Laboratory to a Real Power Plant. *Environmental science & technology* **2010,** *44*, 9207-9212; (b) Pattle, R., Production of electric power by mixing fresh and salt water in the hydroelectric pile. **1954,** *174*, 660; (c) Veerman, J.; Saakes, M.; Metz, S.; Harmsen, G., Reverse electrodialysis: Performance of a stack with 50 cells on the mixing of sea and river water. *J Membrane Sci* **2009,** *327* (1-2), 136-144; (d) Dlugolecki, P.; Gambier, A.; Nijmeijer, K.; Wessling, M., Practical potential of reverse electrodialysis as process for sustainable energy generation. *Environmental science & technology* **2009,** *43* (17), 6888-6894.

24. (a) Veerman, J.; Saakes, M.; Metz, S.; Harmsen, G., Reverse electrodialysis: evaluation of suitable electrode systems. *Journal of Applied Electrochemistry* **2010,** *40* (8), 1461-1474; (b) Veerman, J.; Post, J.; Saakes, M.; Metz, S.; Harmsen, G., Reducing power losses caused by ionic

shortcut currents in reverse electrodialysis stacks by a validated model. *J Membrane Sci* **2008,** *310* (1-2), 418-430.
25. Kontturi, K., Murtomäki, L., Manzanares, J. A., *Ionic Transport Processes in Electrochemistry and Membrane Science*. Oxford University Press: 2008.
26. Sata, T., *Ion Exchange Membranes: Preparation, Characterization, Modification and Application*. Cambridge: 2004.
27. (a) Zhang, M.; Kim, H. K.; Chalkova, E.; Mark, F.; Lvov, S. N.; Chung, T. M., New polyethylene based anion exchange membranes (PE–AEMs) with high ionic conductivity. *Macromolecules* **2011,** *44* (15), 5937-5946; (b) Xu, T. W., Ion exchange membranes: State of their development and perspective. *J Membrane Sci* **2005,** *263* (1-2), 1-29.
28. Xu, T. W.; Yang, W. H.; He, B. L., Effect of solvent composition on the sulfonation degree of poly(phenylene oxide) (PPO). *Chinese Journal of Polymer Science* **2002,** *20* (1), 53-57.
29. Komkova, E. N.; Stamatialis, D. F.; Strathmann, H.; Wessling, M., Anion-exchange membranes containing diamines: preparation and stability in alkaline solution. *J Membrane Sci* **2004,** *244* (1–2), 25-34.
30. Yee, R. S. L.; Rozendal, R. A.; Zhang, K.; Ladewig, B. P., Cost effective cation exchange membranes: A review. *Chem. Eng. Res. Des.* **2012,** *90* (7), 950-959.
31. Guler, E.; Elizen, R.; Vermaas, D.; Saakes, M.; Nijmeijer, K., Performance-determining membrane properties in reverse electrodialysis. *J Membrane Sci* **2013**.
32. (a) Hong, J. G.; Zhang, W.; Luo, J.; Chen, Y., Modeling of power generation from the mixing of simulated saline and freshwater with a reverse electrodialysis system: The effect of monovalent and multivalent ions. *Applied Energy* **2013,** *110*, 244-251; (b) Post, J. W.; Hamelers, H. V. M.; Buisman, C. J. N., Influence of multivalent ions on power production from mixing salt and fresh water with a reverse electrodialysis system. *J Membrane Sci* **2009,** *330* (1-2), 65-72.
33. Güler, E.; van Baak, W.; Saakes, M.; Nijmeijer, K., Monovalent-ion-selective membranes for reverse electrodialysis. *Journal of Membrane Science* **2014,** *455*, 254-270.
34. (a) Klaysom, C.; Marschall, R.; Wang, L. Z.; Ladewig, B. P.; Lu, G. Q. M., Synthesis of composite ion-exchange membranes and their electrochemical properties for desalination applications. *Journal of Materials Chemistry* **2010,** *20* (22), 4669-4674; (b) Wu, Z.; Sun, G.; Jin, W.; Hou, H.; Wang, S.; Xin, Q., Nafion and nano-size TiO2–SO4_2−solid superacid composite membrane for direct methanol fuel cell. *J Membrane Sci* **2008,** *313* (1), 336-343.
35. Wu, Y.; Wu, C.; Xu, T.; Lin, X.; Fu, Y., Novel silica/poly(2,6-dimethyl-1,4-phenylene oxide) hybrid anion-exchange membranes for alkaline fuel cells: Effect of heat treatment. *Journal of Membrane Science* **2009,** *338* (1–2), 51-60.
36. Yang, C. C.; Chiu, S. J.; Chien, W. C.; Chiu, S. S., Quaternized poly(vinyl alcohol)/alumina composite polymer membranes for alkaline direct methanol fuel cells. *Journal of Power Sources* **2010,** *195* (8), 2212-2219.
37. Wang, Z.; Tang, H. L.; Zhang, H. J.; Lei, M.; Chen, R.; Xiao, P.; Pan, M., Synthesis of Nafion/CeO2 hybrid for chemically durable proton exchange membrane of fuel cell. *J Membrane Sci* **2012,** *421*, 201-210.
38. Arsalan, M.; Khan, M. M. A.; Rafiuddin, A comparative study of theoretical, electrochemical and ionic transport through PVC based Cu-3(PO4)(2) and polystyrene supported Ni-3(PO4)(2) composite ion exchange porous membranes. *Desalination* **2013,** *318*, 97-106.
39. Hosseini, S. M.; Madaeni, S. S.; Heidari, A. R.; Amirimehr, A., Preparation and characterization of ion-selective polyvinyl chloride based heterogeneous cation exchange membrane modified by magnetic iron-nickel oxide nanoparticles. *Desalination* **2012,** *284*, 191-199.

40. Yun, S.; Im, H.; Heo, Y.; Kim, J., Crosslinked sulfonated poly(vinyl alcohol)/sulfonated multi-walled carbon nanotubes nanocomposite membranes for direct methanol fuel cells. *J Membrane Sci* **2011,** *380* (1-2), 208-215.
41. Wu, Y.; Wu, C.; Xu, T.; Lin, X.; Fu, Y., Novel silica/poly(2,6-dimethyl-1,4-phenylene oxide) hybrid anion-exchange membranes for alkaline fuel cells: Effect of heat treatment. *J Membrane Sci* **2009,** *338* (1-2), 51-60.
42. Nagarale, R. K.; Shahi, V. K.; Rangarajan, R., Preparation of polyvinyl alcohol-silica hybrid heterogeneous anion-exchange membranes by sol-gel method and their characterization. *J Membrane Sci* **2005,** *248* (1-2), 37-44.
43. Jeong, Y. G.; Park, H. S.; Seo, D. W.; Choi, S. W.; Kim, W. G., Nano Composite Membranes of Sulfonated Poly (2, 6-Dimethyl-1, 4-Phenylene Oxide)/Poly (2, 6-Diphenyl-1, 4-Phenylene Oxide) Copolymer and SiO2 for Fuel Cell Application. *Advanced Materials Research* **2007,** *26*, 835-838.
44. Nagarale, R. K.; Gohil, G. S.; Shahi, V. K.; Rangarajan, R., Organic-inorganic hybrid membrane: Thermally stable cation-exchange membrane prepared by the sol-gel method. *Macromolecules* **2004,** *37* (26), 10023-10030.
45. Tripathi, B. P.; Shahi, V. K., Organic-inorganic nanocomposite polymer electrolyte membranes for fuel cell applications. *Progress in Polymer Science* **2011,** *36* (7), 945-979.
46. Wu, Y. H.; Hao, J. W.; Wu, C. M.; Mao, F. L.; Xu, T. W., Cation exchange PVA/SPPO/SiO2 membranes with double organic phases for alkali recovery. *J Membrane Sci* **2012,** *423*, 383-391.
47. Zuo, X. T.; Yu, S. L.; Xu, X.; Bao, R. L.; Xu, J.; Qu, W. M., Preparation of organic-inorganic hybrid cation-exchange membranes via blending method and their electrochemical characterization. *J Membrane Sci* **2009,** *328* (1-2), 23-30.
48. Wang, F. H.; Lu, Z.; Zhu, H.; Zhang, X. W.; Guo, Z. J.; Wei, Y. S., Preparation and Characterization of Nafion/Sulfonated SiO2 Molecular Sieve Composite Membranes. *Composite Interfaces* **2011,** *18* (3), 237-249.
49. Ke, C. C.; Li, X. J.; Shen, Q. A.; Qu, S. G.; Shao, Z. G.; Yi, B. L., Investigation on sulfuric acid sulfonation of in-situ sol-gel derived Nafion/SiO2 composite membrane. *International Journal of Hydrogen Energy* **2011,** *36* (5), 3606-3613.
50. Kim, J. Y.; Mulmi, S.; Lee, C. H.; Park, H. B.; Chung, Y. S.; Lee, Y. M., Preparation of organic–inorganic nanocomposite membrane using a reactive polymeric dispersant and compatibilizer: Proton and methanol transport with respect to nano-phase separated structure. *J Membrane Sci* **2006,** *283* (1–2), 172-181.
51. Wu, C. M.; Xu, T. W.; Gong, M.; Yang, W. H., Synthesis and characterizations of new negatively charged organic-inorganic hybrid materials Part II. Membrane preparation and characterizations. *J Membrane Sci* **2005,** *247* (1-2), 111-118.
52. Rahimpour, A.; Madaeni, S. S.; Taheri, A. H.; Mansourpanah, Y., Coupling TiO2 nanoparticles with UV irradiation for modification of polyethersulfone ultrafiltration membranes. *J Membrane Sci* **2008,** *313* (1-2), 158-169.
53. Li, J. F.; Xu, Z. L.; Yang, H.; Yu, L. Y.; Liu, M., Effect of TiO2 nanoparticles on the surface morphology and performance of microporous PES membrane. *Applied Surface Science* **2009,** *255* (9), 4725-4732.
54. Wu, Z.; Sun, G.; Jin, W.; Hou, H.; Wang, S.; Xin, Q., Nafion® and nano-size TiO2–SO42− solid superacid composite membrane for direct methanol fuel cell. *J Membrane Sci* **2008,** *313* (1), 336-343.
55. Baglio, V.; Arico, A. S.; Di Blasi, A.; Antonucci, V.; Antonucci, P. L.; Licoccia, S.; Traversa, E.; Fiory, F. S., Nafion-TiO2 composite DMFC membranes: physico-chemical properties of the filler versus electrochemical performance. *Electrochimica Acta* **2005,** *50* (5), 1241-1246.

56. Sairam, M.; Patil, M. B.; Veerapur, R. S.; Patil, S. A.; Aminabhavi, T. M., Novel dense poly(vinyl alcohol)-TiO2 mixed matrix membranes for pervaporation separation of water-isopropanol mixtures at 30 degrees C. *J Membrane Sci* **2006,** *281* (1-2), 95-102.
57. Li, W.; Sun, X.; Wen, C.; Lu, H.; Wang, Z., Preparation and characterization of poly (vinylidene fluoride)/TiO2 hybrid membranes. *Frontiers of Environmental Science & Engineering* **2013,** *7* (4), 492-502.
58. Pourjafar, S.; Rahimpour, A.; Jahanshahi, M., Synthesis and characterization of PVA/PES thin film composite nanofiltration membrane modified with TiO2 nanoparticles for better performance and surface properties. *Journal of Industrial and Engineering Chemistry* **2012,** *18* (4), 1398-1405.
59. Apichatachutapan, W.; Moore, R.; Mauritz, K. A., Asymmetric nafion/(zirconium oxide) hybrid membranes via in situ sol-gel chemistry. *Journal of applied polymer science* **1996,** *62* (2), 417-426.
60. Zhai, Y. F.; Zhang, H. M.; Hu, J. W.; Yi, B. L., Preparation and characterization of sulfated zirconia(SO42-/ZrO2)/Nafion composite membranes for PEMFC operation at high temperature/low humidity. *J Membrane Sci* **2006,** *280* (1-2), 148-155.
61. Siracusano, S.; Baglio, V.; Navarra, M.; Panero, S.; Antonucci, V.; Aricò, A., Investigation of Composite Nafion/Sulfated Zirconia Membrane for Solid Polymer Electrolyte Electrolyzer Applications. *International Journal of Electrochemical Science* **2012,** *7* (2).
62. Bottino, A.; Capannelli, G.; Comite, A., Preparation and characterization of novel porous PVDF-ZrO2 composite membranes. *Desalination* **2002,** *146* (1-3), 35-40.
63. Sacca, A.; Gatto, I.; Carbone, A.; Pedicini, R.; Passalacqua, E., ZrO< sub> 2</sub>–Nafion composite membranes for polymer electrolyte fuel cells (PEFCs) at intermediate temperature. *Journal of power sources* **2006,** *163* (1), 47-51.
64. Navarra, M. A.; Abbati, C.; Croce, F.; Scrosati, B., Temperature-dependent Performances of a Fuel Cell Using a Superacid Zirconia-doped Nafion Polymer Electrolyte. *Fuel Cells* **2009,** *9* (3), 222-225.
65. Vermaas, D. A.; Saakes, M.; Nijmeijer, K., Power generation using profiled membranes in reverse electrodialysis. *J Membrane Sci* **2011,** *385-386*, 234-242.
66. Xu, T. W.; Wu, D.; Wu, L., Poly(2,6-dimethyl-1,4-phenylene oxide) (PPO)-A versatile starting polymer for proton conductive membranes (PCMs). *Progress in Polymer Science* **2008,** *33* (9), 894-915.
67. (a) Aouadj, S.; Chapiro, A., Preparation of hydrophilic membranes by grafting acrylic acid onto pre-irradiated teflon-FEP films. *Die Angewandte Makromolekulare Chemie* **1996,** *235* (1), 73-80; (b) Xu, T. W.; Yang, W. H.; He, B. L., Ionic conductivity threshold in sulfonated poly (phenylene oxide) matrices: a combination of three-phase model and percolation theory. *Chemical Engineering Science* **2001,** *56* (18), 5343-5350.
68. Nagarale, R. K.; Gohil, G. S.; Shahi, V. K., Recent developments on ion-exchange membranes and electro-membrane processes. *Advances in Colloid and Interface Science* **2006,** *119* (2-3), 97-130.
69. Guler, E.; Zhang, Y. L.; Saakes, M.; Nijmeijer, K., Tailor-Made Anion-Exchange Membranes for Salinity Gradient Power Generation Using Reverse Electrodialysis. *Chemsuschem* **2012,** *5* (11), 2262-2270.
70. Lawrence K. Wang, Y.-T. H., Nazih K. Shammas, Advanced Physicochemical Treatment Processes. Springer Science & Business Media: 2007; p. 712.
71. Hong, J. G.; Chen, Y., Evaluation of electrochemical properties and reverse electrodialysis performance for porous cation exchange membranes with sulfate-functionalized iron oxide. *J Membrane Sci* **2015,** *473* (0), 210-217.

72. Klaysom, C.; Moon, S. H.; Ladewig, B. P.; Lu, G. Q. M.; Wang, L. Z., The Influence of Inorganic Filler Particle Size on Composite Ion-Exchange Membranes for Desalination. *Journal of Physical Chemistry C* **2011,** *115* (31), 15124-15132.